NTNU
Norwegian University of
Science and Technology

Experimental Mueller Matrix Images of Liquid Crystalline Domains in Synthetic Clay Dispersions.

Erik Bjørge Theisen

Master of Science in Physics and Mathematics
Submission date: July 2011
Supervisor: Morten Kildemo, IFY

Norwegian University of Science and Technology
Department of Physics

NTNU
Faculty of Natural Sciences
and Technology
Department of Physics

MASTER'S THESIS FOR

Erik Bjørge Theisen

Master of Science in Technology, Applied Physics and Mathematics,
Study Direction Technical Physics

Experimental Mueller Matrix Images of Liquid Crystalline Domains in Synthetic Clay Dispersions.

This work has been carried out under the supervision of Professor Morten Kildemo at the Department of Physics.

Trondheim, July 19, 2011

Abstract

This report is a study of how polarized light can improve our understandings of physical phenomena, such as local organization of anisometric nanoparticles dispersed in a liquid.
The first part of the thesis considers the theoretical aspects of polarized light. The Maxwell's equations are considered together with the Stokes formalism and the Mueller matrix. The Mueller matrix is analyzed in depth by looking at different ways it can be decomposed into several matrices, each clearly representing the physical phenomena of depolarization, diattenuation and retardance. The physics behind the phenomena will then be shortly addressed.
The second part of the thesis describes the Mueller Matrix Imaging (MMI) ellipsometer, developed in the Applied Optics Group at NTNU. The results of Mueller imaging of air will be presented and discussed in order to get more understanding of the ellipsometer.
The third and main part of the thesis, focuses on applying the MMI ellipsometer in order to study complex phenomena in clay dispersion. By looking at the development of samples of aqueous clay dispersions, the creation of different phases will be recorded. Some of those phases have crystalline properties and a Mueller matrix imaging can reveal much about its structure. A decomposition of the Mueller matrix can tell even more about the properties of the phases.

Contents

1 Introduction

1.1 Decomposition of Mueller matrices

Mueller matrices where developed in 1943 by Hans Mueller [1]. In the following 70 years it has proved to be a good tool in order to understand how light, represented by the Stokes vector, are manipulated by the surrounding media. This have been exploited among others in examination of biological tissue [11], where the interaction between the biological media and light has been exploited in order to describe the tissue. The Mueller calculus has anyway one obvious drawback, usually it has no clear physical interpretation. In the nineties this problem was approached by decomposing the Mueller matrix in three different matrices, where each matrix is describing either the depolarizing, the diattenuation or the retardance effect of the Mueller matrix [3]. By doing this one can quickly give a physical interpretation of how a Mueller matrix will affect a Stokes vector. In the last 15 years, several product decompositions has been presented, where the number of matrices and the their internal placements have varied [6]. The decomposition of the Mueller matrix has a wide range of potentials, among others to reveal the structure of clay dispersion.

2 Motivation

The Department of Applied Physics at NTNU is working with the challenges of describing the different phases of clay dispersions. In several years the Complex Systems and Soft Materials Group has been addressing those problems by using among others X-ray scanning. Recently the Applied Optics Group have been involved, because of their knowledge of how the optical properties of material can be used to reveal information about its structure.
The benefits of an improved understanding of clay are enormous. Clay is one of the most abundant materials at the surface of earth. This causes headache for construction engineer when they have to build at quick clay, which threatens to collapse under the right circumstances [19]. Even at the bottom of the sea, a better understanding of clay can be important. Huge amounts of oil are pumped up from a clay rich seabed outside Norway. In addition there has been some speculations recently that pumping down CO_2 in the same seabed could reduce the CO_2 concentration in the atmosphere [16]. Such an idea requires that one understands how to trap the CO_2 molecules within clay.
A better understanding of clay could also be important because the clay particles have showed some remarkable abilities of self-organizing [17], [18]. The sheer number of molecules nanotechnology has to handle has challenged the progress of the technology. If the molecules could organize themselves nanotechnology could finally be a part of everyday life, as science fiction has promised us for years.

2.1 The contribution of this thesis

The author's part of this work is that he will experimentally investigate how aqueous dispersions of clay form phases with the help of gravity. In order to do this a Mueller Matrix Imaging ellipsometer will be used. In order to use the results from the ellipsometer, a good understanding of the theory behind the matrix method for manipulating Stokes vectors is needed. The concept of decomposing the Mueller matrix is explored, leading to matrices representing the phenomena of retardance, diattenuation and depolarization.
Before the results of ellipsometer can be presented, a basic understanding of the instrument is required. This will be done in section 5.1, together with Mueller matrix imaging of air. Air is a good start to investigate the properties of the ellipsometer.
In the last part of the thesis both the theoretical aspects and experimental results of aqueous dispersion of clay will be considered. The anisotropy of some of the phases in the dispersion will be exploited in order to understand how the clay particles interact with each other, liquids to liquids interfaces and the walls of the container.

3 Polarization of light

3.1 Background

The content in this subsection is mainly based on chapter 2 of Bohren and Huffman [2].

3.1.1 Maxwell's equations

The four Maxwell's equations in a linear, isotropic and homogenous medium:

$$\nabla \cdot \mathbf{D} = \rho_F \tag{1}$$

$$\nabla \cdot \mathbf{B} = 0 \tag{2}$$

$$\nabla \times \mathbf{E} + \frac{\partial \mathbf{B}}{\partial t} = 0 \tag{3}$$

$$\nabla \times \mathbf{H} = \mathbf{J_F} + \frac{\partial \mathbf{D}}{\partial t} \tag{4}$$

Here $\mathbf{E}$ is the electric field, $\mathbf{B}$ is the magnetic induction, $\mathbf{D}$ is the electric displacement, $\mathbf{H}$ is the magnetic field while $\mathbf{J_F}$ is the free current density. $\mathbf{D}$, $\mathbf{H}$, $\mathbf{J_F}$ and $\mathbf{B}$ are defined by:

$$\mathbf{D} = \epsilon_0 \mathbf{E} + \epsilon_0 \chi \mathbf{E} \tag{5}$$

$$\mathbf{H} = \frac{\mathbf{B}}{\mu_0} - \mathbf{M} \tag{6}$$

$$\mathbf{J_F} = \sigma \mathbf{E} \tag{7}$$

$$\mathbf{B} = \mu \mathbf{H} \tag{8}$$

Where the coefficients are tabulated in table 1.

Table 1: Coefficients of the Maxwell equations

Coefficient	Meaning
ρ_f	charge density of the media
ϵ_0	permittivity of vacuum
ϵ	permittivity of the media
μ_0	permeability of vacuum
μ	permeability of the media
$\mathbf{M}$	the magnetization of the media
σ	conductivity of the media
χ	the electric susceptibility of the media

A solution for $\mathbf{E}$ of the Maxwell's equations is:

$$\mathbf{E} = E_{\parallel 0}(t)\cos(\mathbf{kz} + i\omega t + \delta_{\parallel}(t))\widehat{\mathbf{e}}_{\parallel} + E_{\perp 0}(t)\cos(\mathbf{kz} + i\omega t + \delta_{\perp}(t))\widehat{\mathbf{e}}_{\perp} \tag{9}$$

The direction of the wave is in the $\widehat{\mathbf{z}}$ direction, while $\widehat{\mathbf{e}}_{\parallel}$ and $\widehat{\mathbf{e}}_{\perp}$ are perpendicular to $\widehat{\mathbf{z}}$. $\mathbf{k}$ is the wave vector, ω is the frequency of the electromagnetic wave, $E_{\parallel 0}(t)$ and $E_{\perp 0}(t)$ are the instantaneous amplitudes, while $\delta_{\perp}$(t) and $\delta_{\parallel}$(t) are the instantaneous phase factors.

3.2 The Stokes vector and the scattering Mueller matrix

The topic of general Mueller matrices and how they manipulate Stokes vectors will only be shortly addressed. A comprehensive study is given in Goldstein [1].

The Stoke formalism can represent every possible polarization state of the light and it consists of four parameters in a column matrix:

$$S = \begin{pmatrix} I \\ Q \\ U \\ V \end{pmatrix}$$

If $z = 0$, equations (9) can be used, with the help of time averaging and trigonometric relations, to show that the Stokes vector can be defined as:

$$\begin{pmatrix} I \\ Q \\ U \\ V \end{pmatrix} = \begin{pmatrix} \langle E_{\parallel s} E^*_{\parallel s} + E_{\perp s} E^*_{\perp s} \rangle \\ \langle E_{\parallel s} E^*_{\parallel s} - E_{\perp s} E^*_{\perp s} \rangle \\ \langle E_{\parallel s} E^*_{\perp s} + E_{\perp s} E^*_{\parallel s} \rangle \\ i\langle E_{\parallel s} E^*_{\perp s} - E_{\perp s} E^*_{\parallel s} \rangle \end{pmatrix} \tag{10}$$

Here $\langle\rangle$ means time averaging and * means complex conjugate.
By using equation (10), different states of light can be represented. An example is light that is polarized linearly in the $\hat{\mathbf{e}}_{\parallel}$ direction with a total intensity of I_0. Then $E_{\perp}$=0, $I_0 = E^2_{\parallel}$ and the Stokes vector is:

$$S = I_0 \begin{pmatrix} 1 \\ 1 \\ 0 \\ 0 \end{pmatrix}$$

Another example is right-circularly polarized light, where $E_{\parallel} = E_{\perp} = E_0$, $I_0 = 2E^2_0$ and the Stokes vector is:

$$S = I_0 \begin{pmatrix} 1 \\ 0 \\ 0 \\ 1 \end{pmatrix}$$

Another property of the Stokes vector is that it can represent partly depolarized light. For completely polarized light I, the intensity of the light, can be written:

$$I^2 = Q^2 + U^2 + V^2$$

The degree of polarization of the light can be found by using:

$$\frac{\sqrt{Q^2 + U^2 + V^2}}{I}$$

If the light is completely unpolarized, then $Q = U = V = 0$.
An important use of the Stokes vector is together with the Mueller matrix. The Mueller matrix can describe the effect of surrounding media on the polarization state of light. It is a 4×4 matrix that multiplied with a Stokes vector gives a new Stokes vector:

$$S_{new} = \mathbf{M} S_{old} \tag{11}$$

Here $\mathbf{M}$ is:

$$\begin{pmatrix} m_{11} & m_{12} & m_{13} & m_{14} \\ m_{21} & m_{22} & m_{23} & m_{24} \\ m_{31} & m_{32} & m_{33} & m_{34} \\ m_{41} & m_{42} & m_{43} & m_{44} \end{pmatrix} \tag{12}$$

The challenge is to give values to all the elements of $\mathbf{M}$ for different problems. In some rare cases, like Mie theory [2], the elements can be found analytically, but usually they have to be decided experimentally.

3.3 Examples of different Mueller matrices

The examples of different Mueller matrix given in this subsection are diattenuator, retarder and depolarizer. The work is based upon Goldstein [1], where a more complete study is given.

3.3.1 Diattenuator

A diattenuator changes the amplitude of two orthogonal field components of the incoming light in different ways. If x and y are the two orthogonal axes, where p_x and p_y are their amplitude coefficients, it can be showed that the corresponding Mueller matrix can be written like:

$$\begin{pmatrix} I' \\ Q' \\ U' \\ V' \end{pmatrix} = \frac{1}{2} \begin{pmatrix} p_x^2 + p_y^2 & p_x^2 - p_y^2 & 0 & 0 \\ p_x^2 - p_y^2 & p_x^2 + p_y^2 & 0 & 0 \\ 0 & 0 & 2p_x p_y & 0 \\ 0 & 0 & 0 & 2p_x p_y \end{pmatrix} \begin{pmatrix} I \\ Q \\ U \\ V \end{pmatrix} \tag{13}$$

If $p_x = p_y = p$ equation (13) simplifies to a neutral density filter.
A diattenuator can be used as a polarizer. For example it can be showed by setting $p_x = 1$ and $p_y = 0$ in equation (13) that the emerging light is completely polarized in the x-direction.

3.3.2 Retarder

A retarder changes the phases of two orthogonal axes of the incoming light in different ways. If x and y are two orthogonal axes and the retarder introduce a phase shift of ϕ, the change of the incoming light, $E(z,t)$, can be written like:

$$E'_x(z,t) = e^{+i\phi/2} E_x(z,t)$$

$$E'_y(z,t) = e^{-i\phi/2} E_y(z,t)$$

Here the x axis is the fast and y is the slow axis.
It can be showed that the Mueller matrix of a retarder can be written like equation (14).

$$\begin{pmatrix} I' \\ Q' \\ U' \\ V' \end{pmatrix} = \begin{pmatrix} 1 & 0 & 0 & 0 \\ 0 & 1 & 0 & 0 \\ 0 & 0 & \cos\phi & \sin\phi \\ 0 & 0 & -\sin\phi & \cos\phi \end{pmatrix} \begin{pmatrix} I \\ Q \\ U \\ V \end{pmatrix} \tag{14}$$

3.3.3 Depolarizer

If energy goes from polarized states to the unpolarized state in an interaction between the light and the surroundings, it is depolarization. A Mueller matrix of a depolarizer can be written like:

$$\begin{pmatrix} I' \\ Q' \\ U' \\ V' \end{pmatrix} = \begin{pmatrix} 1 & 0 & 0 & 0 \\ 0 & a & 0 & 0 \\ 0 & 0 & b & 0 \\ 0 & 0 & 0 & c \end{pmatrix} \begin{pmatrix} I \\ Q \\ U \\ V \end{pmatrix} \tag{15}$$

where $|a|, |b|, |c| \leq 1$. In this process $I' = I$ so the total intensity of the light is not changed, while the other elements of the Stokes vector of equation (15) is changed. The average of the depolarization is given by:

$$\Delta = 1 - \frac{|a| + |b| + |c|}{3} \tag{16}$$

If a, b and c is 1, equation (15) reduces to a pure transition matrix that does not change the Stokes vector.
Equation (15) is only one way to represent a depolarizer. Other matrices can also be used, like the one in forward decomposition.

3.4 Decomposition of a depolarizing Mueller matrix

One drawback of Mueller matrix in the form of equation (12) is that often the matrix will have no obvious physical interpretation. In this subsection different methods of decomposing Mueller matrices are presented. The idea will be to isolate every effect, like depolarization, retardance and diattenuation in their own matrices. This can be done by decomposing **M** into three or more different matrices. The resulting matrices will have a clear physical interpretation corresponding to the different matrices discussed in subsection 3.3. This text is based on the work of Lu and Chipman [3], Morio and Goudail [4], Manhas et. al. [5] and Ossikovski [8].

3.4.1 Notation

The start of decomposition is to cast **M** into the following form

$$\mathbf{M} = m_{11} \begin{pmatrix} 1 & \overrightarrow{D}^T \\ \overrightarrow{P} & \mathbf{m} \end{pmatrix}$$

where $\overrightarrow{P}$ is the polarisance vector given by

$$\overrightarrow{P} = \frac{1}{m_{11}}[m_{21} \quad m_{31} \quad m_{41}]^T \tag{17}$$

$\overrightarrow{D}$ is the diattenuation vector given by

$$\overrightarrow{D} = \frac{1}{m_{11}}[m_{12} \quad m_{13} \quad m_{14}]^T \tag{18}$$

and **m** is a 3×3 matrix given by:

$$\mathbf{m} = \frac{1}{m_{11}} \begin{pmatrix} m_{22} & m_{23} & m_{24} \\ m_{32} & m_{33} & m_{34} \\ m_{42} & m_{43} & m_{44} \end{pmatrix}$$

In the rest of this subsection the notation of Morio and Goudail [4] will be followed. 4×4 matrices will be denoted by bold capital letters, 3×3 matrices with bold lowercase letters and 3×1 matrices with numbers or italic capital letters with an arrow.

The Mueller matrix $\mathbf{M}$ will be divided into three kinds of matrices: $\mathbf{M_\Delta}$, $\mathbf{M_R}$ and $\mathbf{M_D}$, representing the depolarization, retardance and diattenuation part of $\mathbf{M}$ respectively.

3.4.2 Forward decomposition

The idea behind forward decomposition [3] is to decompose $\mathbf{M}$ into three matrices:

$$\mathbf{M} = \mathbf{M_\Delta M_R M_D}. \tag{19}$$

In order to find the different matrices, one start with the definition of $\mathbf{M_D}$:

$$\mathbf{M_D} = T_u \begin{pmatrix} 1 & \overrightarrow{D}^T \\ \overrightarrow{D} & \mathbf{m_D} \end{pmatrix}$$

where T_u is the unpolarized light transmittance, $\overrightarrow{D}$ is given by equation (18) and $\mathbf{m_D}$ is:

$$\mathbf{m_D} = \sqrt{1-D^2}I + (1-\sqrt{1-D^2})\frac{\overrightarrow{D}\overrightarrow{D}^T}{|\overrightarrow{D}|^2}.$$

I is the 3×3 identity matrix.
$\mathbf{M_\Delta}$ is given by

$$\mathbf{M_\Delta} = \begin{pmatrix} 1 & \overrightarrow{0}^T \\ \overrightarrow{P_\Delta} & \mathbf{m_\Delta} \end{pmatrix}$$

where $\overrightarrow{P_\Delta}$ is given by:

$$\overrightarrow{P_\Delta} = \frac{\overrightarrow{P} - \mathbf{m}\overrightarrow{D}}{1-D^2}$$

$\mathbf{M_R}$ is given by:

$$\mathbf{M_R} = \begin{pmatrix} 1 & \overrightarrow{0}^T \\ \overrightarrow{0} & \mathbf{m_R} \end{pmatrix}$$

where $\mathbf{m_R}$ is given by:

$$\mathbf{m_R} = \frac{1}{a}(\mathbf{m} - 1) + \frac{\overrightarrow{P}\overrightarrow{D}}{|P||D|} \tag{20}$$

where $a = \sqrt{1 - \overrightarrow{D}^2)}$. $\mathbf{M_R}$ can be expressed like:

$$\mathbf{M_R} = \begin{pmatrix} 1 & 0 & 0 & 0 \\ 0 & \cos^2(2\theta) + \sin^2(2\theta)\cos(\delta) & \cos(2\theta)\sin(2\theta)(1 - \cos(\delta)) & -\sin(2\theta)\sin(\delta) \\ 0 & \cos(2\theta)\sin(2\theta)(1 - \cos(\delta)) & \sin^2(2\theta) + \cos^2(2\theta)\cos(\delta) & \cos(2\theta)\sin(\delta) \\ 0 & \sin(2\theta)\sin(\delta) & -\cos(2\theta)\sin(\delta) & \cos(\delta) \end{pmatrix}$$

$$\times \begin{pmatrix} 1 & 0 & 0 & 0 \\ 0 & \cos(2\Psi) & \sin(2\Psi) & 0 \\ 0 & -\sin(2\Psi) & \cos(2\Psi) & 0 \\ 0 & 0 & 0 & 1 \end{pmatrix} \tag{21}$$

δ is linear retardance, θ is the orientation of fast axis of the linear retarder and Ψ is the optical rotation. A thorough definition can be found in Hauge et al. [13].
In order to find the different parameters of retardance, the retardance vector $\overrightarrow{R} = [1, r_1, r_2, r_3]$ can be used. Its elements can be found by using:

$$r_i = \frac{1}{2\sin R} \sum_{j,k=1}^{3} \varepsilon_{ijk}(\mathbf{m_R})_{jk}$$

where R, the total retardance, is given by:

$$R = \cos^{-1}\{\frac{tr(\mathbf{M_R})}{2} - 1\} = \cos^{-1}\{2\cos^2(\Psi)\cos^2(\frac{\delta}{2}) - 1\} \tag{22}$$

The last expression for R is found by using equation (21).
Now δ, θ and Ψ can be found with the help of R and $\overrightarrow{R}$:

$$\delta = 2\cos^{-1}\{\sqrt{r_3^2(1 - \cos^2(R/2)) + \cos^2(R/2}\} \tag{23}$$

$$\Psi = \cos^{-1}\{\frac{\cos(R/2)}{\cos(\delta/2)}\} \tag{24}$$

$$\theta = \frac{1}{2}\tan^{-1}(r_2/r_1) \tag{25}$$

3.4.3 Symmetric decomposition

Symmetric decomposition [8] places the depolarization matrix in the center, with a retardance and a diattenuation matrix at each side:

$$\mathbf{M} = \mathbf{M_2}\mathbf{M_{\Delta d}}\mathbf{M_1^T} = \mathbf{M_{D2}}\mathbf{M_{R2}}\mathbf{M_{\Delta d}}\mathbf{M_{R1}^T}\mathbf{M_{D1}} \tag{26}$$

Here $\mathbf{M_{D1,D2}}$ will be written like:

$$\mathbf{M_{D1,D2}} = T_{u1,u2}\begin{pmatrix} 1 & \overrightarrow{D_{1,2}}^T \\ \overrightarrow{D_{1,2}} & \mathbf{m_{D1,D2}} \end{pmatrix} \tag{27}$$

$\mathbf{M_{R1,R2}}$ will be cast like:

$$\mathbf{M_{R1,R2}} = \begin{pmatrix} 1 & \overrightarrow{0}^T \\ \overrightarrow{0} & \mathbf{m_{R1,R2}} \end{pmatrix} \tag{28}$$

and $\mathbf{M_{\Delta d}}$ will be written like:

$$\mathbf{M_{\Delta d}} = \begin{pmatrix} d_0 & 0 & 0 & 0 \\ 0 & d_1 & 0 & 0 \\ 0 & 0 & d_2 & 0 \\ 0 & 0 & 0 & d_3 \end{pmatrix} \tag{29}$$

The advantage of this decomposition is that $\mathbf{M_{\Delta d}}$ is diagonal. In addition it contains more information of where the retardance and diattenuation is happening in the system. For example, if the retardance is happening before the depolarization it will be obvious in equation (26).

In order to find the different matrices of equation (26) some matrix calculations are required. The start is the diattenuation matrices of $\mathbf{M_{D1}}$ and $\mathbf{M_{D2}}$. By setting $T_u = 1/\sqrt{1-D^2}$ it can be shown:

$$\mathbf{M_D^{-1}} = \mathbf{G}\mathbf{M_D}\mathbf{G} \tag{30}$$

which leads to::

$$(\mathbf{MG})(\mathbf{M_{D1}G}) = \mathbf{M_{D2}}(\mathbf{M_{R2}}\mathbf{M_{\Delta d}}\mathbf{M_{R1}^T}) = \mathbf{M_{D2}}\mathbf{M'} \tag{31}$$

where $\mathbf{G}$ =diag$(1,-1,-1,-1)$ and $\mathbf{M'} = \mathbf{M_{R2}}\mathbf{M_{\Delta d}}\mathbf{M_{R1}^T}$.
By inspection $\mathbf{M'}$ can be written:

$$\mathbf{M'} = \begin{pmatrix} d_0 & \overrightarrow{0}^T \\ \overrightarrow{0} & \mathbf{m'} \end{pmatrix} \tag{32}$$

where d_0 is from the depolarization matrix, equation (29). Because of the two zero vectors, the first columns of both side of equation (31) can be set equal:

$$\mathbf{MG}T_{u1}\begin{pmatrix} 1 \\ \overrightarrow{D_1} \end{pmatrix} = d_0 T_{u2}\begin{pmatrix} 1 \\ \overrightarrow{D_2} \end{pmatrix} \tag{33}$$

By using the same process on $\mathbf{M^T}$ the result is:

$$\mathbf{M^T G}T_{u2}\begin{pmatrix} 1 \\ \overrightarrow{D_2} \end{pmatrix} = d_0 T_{u1}\begin{pmatrix} 1 \\ \overrightarrow{D_1} \end{pmatrix} \tag{34}$$

By combining equation (33) and (34) one ends up with:

$$\mathbf{M^T GMG}\begin{pmatrix} 1 \\ \overrightarrow{D_1} \end{pmatrix} = d_0^2\begin{pmatrix} 1 \\ \overrightarrow{D_1} \end{pmatrix}$$

$$\mathbf{MGM^T G}\begin{pmatrix} 1 \\ \overrightarrow{D_2} \end{pmatrix} = d_0^2\begin{pmatrix} 1 \\ \overrightarrow{D_2} \end{pmatrix}$$

By solving this pair of eigenvalue equations one finds $\overrightarrow{D_1}$ and $\overrightarrow{D_2}$. Then $\mathbf{M_{D1}}$ and $\mathbf{M_{D2}}$ is found by using equation (27).
The next step is to find $\mathbf{M_{R1}}$, $\mathbf{M_{R2}}$ and $\mathbf{M_{\Delta d}}$. By using (30) and (31) it can easily be shown that $\mathbf{M'} = \mathbf{M_{D2}^{-1}} \mathbf{M} \mathbf{M_{D1}^{-1}} = \mathbf{M_{R2}^{-1}} \mathbf{M} \mathbf{M_{R1}^{-1}}$. Because of the two zero vectors of $\mathbf{M_R}$, $\mathbf{m'}$ can be expressed like:

$$\mathbf{m'} = \mathbf{m_{R2}} \mathbf{m_{\Delta d}} \mathbf{m_{R1}^{T}}$$

By using singular-value decomposition of $\mathbf{m}$', one finds $\mathbf{m_{R2}}$, $\mathbf{m_{\Delta d}}$ and $\mathbf{m_{R1}}$. $\mathbf{M_{R1}}$ and $\mathbf{M_{R2}}$ are found by using equation (28).

3.4.4 Other decomposition

There are several other ways to decompose a Mueller matrix. The forward decomposition is just a member of a family of six different ways of decomposing, where the internal placements of $\mathbf{M_R}$, $\mathbf{M_D}$ and $\mathbf{M_\Delta}$ change.
Another member of this family is reverse decomposition:

$$\mathbf{M} = \mathbf{M_D^r} \mathbf{M_R^r} \mathbf{M_\Delta^r}$$

which is discussed in Morio et al. [4] and Ossikovski et al. [6].
In a quite similar way the symmetric decomposition presented in this subsection is just a member of a family of four.
A complete different way of decomposition, called Cloude decomposition, is presented by Ossikovski et al. [6].

$$\mathbf{M} = \lambda_1 \mathbf{M}_1 + \lambda_2 \mathbf{M}_2 + \lambda_3 \mathbf{M}_3 + \lambda_4 \mathbf{M}_4$$

where λ_n is the four eigenvalues of $\mathbf{M}$ and $\mathbf{M_n}$ are four non-depolarizing matrices. This way of decomposition reveals unphysical Mueller matrices since the eigenvalues of a physical realizable are positive. A physical Mueller matrix is characterized by a real 4×4 matrix that for any valid input Stokes vector gives a valid output Stokes vector with equal or lower intensity.

3.4.5 Problems with decompositions

The different ways of Mueller matrix decomposition have drawbacks that have been addressed in some articles.
Morio and Goudail [4] have showed that some decompositions may give raise to unphysical matrices. This is a problem when $\mathbf{M_D}$ is preceded by $\mathbf{M_\Delta}$, like the reverse decomposition.
Another problem arises because matrix multiplication is not a commutative operation, which may result in wrong forms of the $\mathbf{M_D}$, $\mathbf{M_\Delta}$ and $\mathbf{M_R}$ matrices. This has been showed by Ossikovski et. al. [7]. They conducted some simple experiments, where they sent light through a diffuser followed by a diattenuator and finally a retarder. In order to reproduce the Mueller matrix of each component they used both reverse and forward decomposition. They were able to reproduce the Mueller matrix of each component with reverse decomposition, but forward decomposition failed. The reason was the internal placement of the components that favored reverse decomposition. This problem could be avoided by using the symmetric decomposition.

4 The physics behind depolarization, diattenuation and retardance

In this section the physics behind the different phenomena encountered in the previous section will be explained. A more comprehensive study is given by Goldstein [1].

4.1 Multiple scattering

The phenomenon of depolarization can be defined as energy going from a polarized state to an unpolarized state. Multiple scatterings that make a beam of light loose coherence can cause this.

4.2 Anisotropy

Anisotropy is a property of a material that gives raise to many phenomena like diattenuation and retardance. An anisotropic material is characterized by different refractive indices in different spatial directions. Light waves of the same wavelength often experience different refractive index because of different ways of propagation and/or different polarization.
A wide range of materials is inherently anisotropic. Many of them are different crystals, but there is also biological anisotropic materials [11], such as chicken cartilage. A material must have a kind of structure in order to be anisotropic.

4.2.1 Background and theory

The phenomenon of anisotropy is the result of the electric displacement vector $\mathbf{D}$ from Maxwell's equations not being parallel with $\mathbf{E}$. In order to understand what is happening, one needs to rewrite equation (5). χ is not a scalar, but a tensor:

$$\mathbf{D} = \epsilon_0\mathbf{E} + \epsilon_0\chi\mathbf{E} = \epsilon_0\mathbf{E} + \mathbf{P}$$

where $\mathbf{P}$ is the polarization vector that is not parallel to $\mathbf{E}$. By making the assumption that the material is linear, $\mathbf{P}$ can be written:

$$\begin{pmatrix} \mathbf{P}_1 \\ \mathbf{P}_2 \\ \mathbf{P}_3 \end{pmatrix} = \epsilon_0 \begin{pmatrix} \chi_{11} & \chi_{12} & \chi_{13} \\ \chi_{21} & \chi_{22} & \chi_{23} \\ \chi_{31} & \chi_{32} & \chi_{33} \end{pmatrix} \begin{pmatrix} \mathbf{E}_1 \\ \mathbf{E}_2 \\ \mathbf{E}_3 \end{pmatrix}$$

where χ_{ij} is the susceptibility tensor and the indices 1,2,3 are representing the three Cartesian directions.
D and **E** can be related in a similar way:

$$\begin{pmatrix} \mathbf{D}_1 \\ \mathbf{D}_2 \\ \mathbf{D}_3 \end{pmatrix} = \epsilon_0 \begin{pmatrix} 1+\chi_{11} & \chi_{12} & \chi_{13} \\ \chi_{12} & 1+\chi_{22} & \chi_{23} \\ \chi_{13} & \chi_{23} & 1+\chi_{33} \end{pmatrix} \begin{pmatrix} \mathbf{E}_1 \\ \mathbf{E}_2 \\ \mathbf{E}_3 \end{pmatrix} \tag{35}$$

Some important modifications can be obtained by taking a closer look at the susceptibility tensor matrix in equation (35). By exploiting that the matrix is symmetric, it can be rotated to new coordinate axes called the principal axes. The result is a tensor matrix written in a diagonalized form:

$$\begin{pmatrix} \chi'_{11} & 0 & 0 \\ 0 & \chi'_{22} & 0 \\ 0 & 0 & \chi'_{33} \end{pmatrix}$$

where the different χ's are the principal susceptibilities. The principal indices of refraction, $\mathbf{n}_1^2$, $\mathbf{n}_2^2$ and $\mathbf{n}_3^2$, are obtained by using equation (35):

$$\begin{pmatrix} \mathbf{n}_1^2 & 0 & 0 \\ 0 & \mathbf{n}_2^2 & 0 \\ 0 & 0 & \mathbf{n}_3^2 \end{pmatrix} = \begin{pmatrix} 1+\chi'_{11} & 0 & 0 \\ 0 & 1+\chi'_{22} & 0 \\ 0 & 0 & 1+\chi'_{33} \end{pmatrix} \tag{36}$$

If the material is isotropic $\mathbf{n}_1^2 = \mathbf{n}_2^2 = \mathbf{n}_3^2$. Some materials are uniaxial, meaning that $\mathbf{n}_1^2 = \mathbf{n}_2^2 \neq \mathbf{n}_3^2$. Others materials are biaxial, where $\mathbf{n}_1^2 < \mathbf{n}_2^2 < \mathbf{n}_3^2$.

4.2.2 Ordinary and extraordinary axis

When the material is uniaxial the two equal refractive indices of equation (36) are termed the ordinary refractive index, n_o. The last refractive index is termed the extraordinary refractive index, n_e. This is showed in figure 1.

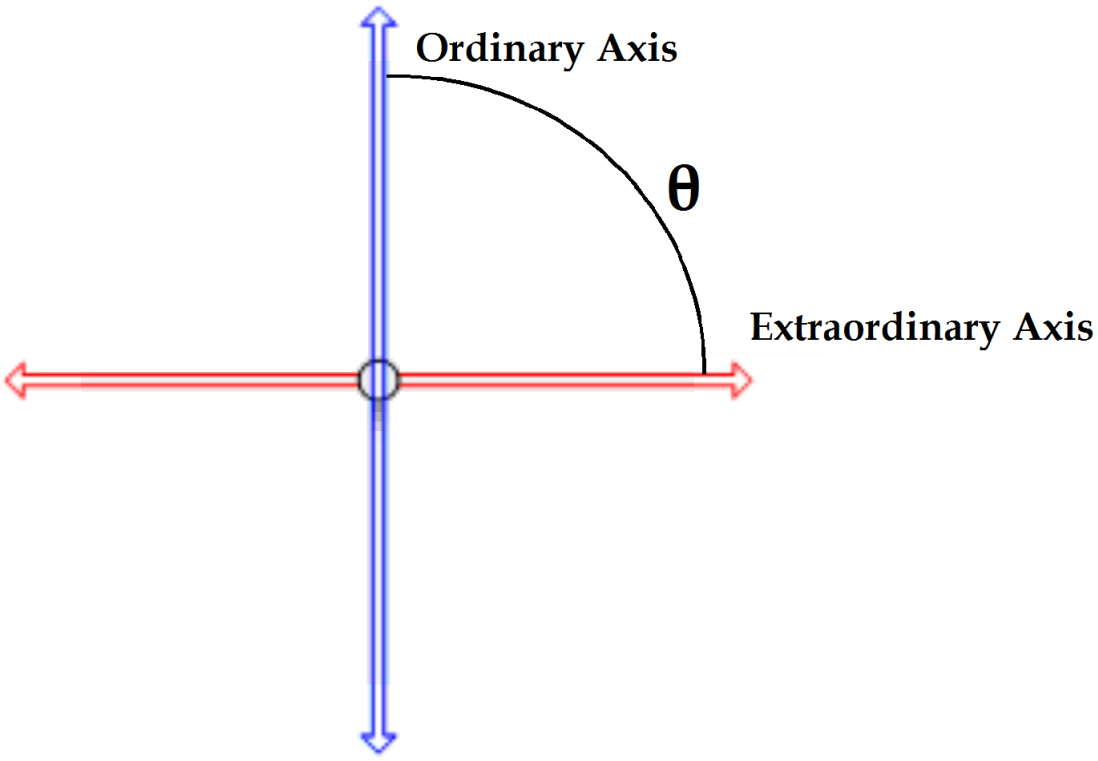

Figure 1: The ordinary and extraordinary axis of a uniaxial material. The refractive index pointing out of the paper is also n_o. θ is showing the orientation of the extraordinary axis.

Whether one gets diattenuation or retardance is a question about the imaginary and real part of the refractive indices. If the imaginary part differs one gets diattenuation, while a different real part results in retardance.

4.2.3 Artificial induced anisotropy

In most anisotropic materials the anisotropy is something inherent that cannot be changed. This is not true about a small, but important class of materials, where the anisotropy can be changed by electric voltage. This makes the basis for modulators that may change the direction of ordinary and extraordinary axis of a uniaxial material. Such modulators can be exploited in order to make a Mueller matrix ellipsometer, such as the MMI instrument that will be presented in the next section.

5 Mueller matrix imaging

5.1 The ellipsometer

The equipment used to obtain the results in the thesis is called a Mueller matrix ellipsometer. It has been developed and improved by the Applied Optics Group in the years 2007-2011. Some of its contributors are Jarle Ladstein, Halvard Olsen Skjerping, Lars Martin Sandvik Aas and Pål Gunnar Ellingsen. A more comprehensive study is given in Ellingsen [11] and Aas et. al. [12].

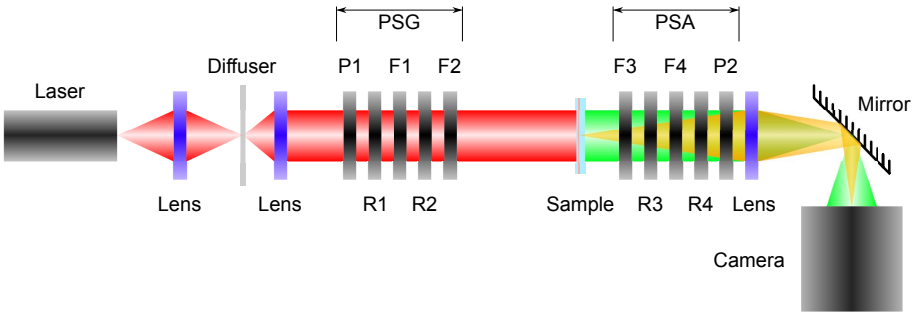

Figure 2: The ellipsometer is passing from left to right. P is a polarizer, R a retarder and F a ferroelectric liquid crystals, a type of modulator. Figure is from [11].

The imaging system consists of several components showed in figure 2. The laser light, with a wavelength of 980 nm, is approaching from the left and is first passing one lens, a diffuser and a lens again in order to give collimated light. Then the light is passing the PSG-component consisting of several subcomponents: one polarizer (P1), two retarders (R1 and R2) and two ferroelectric liquid crystals. The succession of subcomponents experienced by the laser light is P1, R1, F1, R2 and F2. Then the light is passing the sample, the PSA, the mirror and at last the NIR InGaAs camera [10] where the influenced light is recorded, a process that takes 3-4 minutes. The PSA is a mirror of the PSG, consisting of the same subcomponents in reverse order (F3, R3, F4, R4, P2). Ferroelectric liquid crystals are modulators where the fast and slow axis can be rotated by 45^o. By using the different states of the modulators of the ellipsometer it is possible to obtain 16 different intensity measurements of the

sample. Then **B**, an intensity matrix, can be constructed.

$$\mathbf{B} = \begin{pmatrix} B_{11} & B_{12} & B_{13} & B_{14} \\ B_{21} & B_{22} & B_{23} & B_{24} \\ B_{31} & B_{32} & B_{33} & B_{34} \\ B_{41} & B_{42} & B_{43} & B_{44} \end{pmatrix}$$

The subscripts are the different states of the PSG and PSA.
In addition it is possible to define two helping matrices: **A** and **W**. They are defined by:

$$\mathbf{W} = [\overrightarrow{S}_{W1} \quad \overrightarrow{S}_{W2} \quad \overrightarrow{S}_{W3} \quad \overrightarrow{S}_{W4}]$$

and

$$\mathbf{A} = \begin{pmatrix} \overrightarrow{S}_{A1} \\ \overrightarrow{S}_{A2} \\ \overrightarrow{S}_{A3} \\ \overrightarrow{S}_{A4} \end{pmatrix}$$

The different $\overrightarrow{S}$ vectors are obtained with the Mueller matrix of PSG ($\mathbf{M}_{PSG}$) and PSA ($\mathbf{M}_{PSA}$), using the following equations:

$$S_{Ai} = [1 \quad 0 \quad 0 \quad 0]\mathbf{M}_{PSAi} = [m_{11} \quad m_{12} \quad m_{13} \quad m_{14}]_{PSAi}$$

and

$$S_{Wi} = \mathbf{M}_{PSGi} \begin{pmatrix} 1 \\ 0 \\ 0 \\ 0 \end{pmatrix} = \begin{pmatrix} m_{11} \\ m_{21} \\ m_{31} \\ m_{41} \end{pmatrix}_{PSGi}$$

By using **A**, **W** and **M** of the sample it is possible to reconstruct **B**:

$$\mathbf{B} = \mathbf{AMW}.$$

Rewriting this equation leads to an expression for $\mathbf{M}$:

$$\mathbf{M} = \mathbf{A^{-1}BW^{-1}}.$$

5.2 Mueller matrix imaging of air

The simplest sample a Mueller matrix ellipsometer can study is air. Because nothing is between PSA and PSG the resulting Mueller matrix should be the transition matrix of equation (15), where a, b and c is 1. If not, something is wrong. This will be illustrated by some examples.
A good Mueller matrix of air is shown by figure 3. Notice that the Mueller matrix is actually a collection of many Mueller matrices, in this case about 328 000 matrices. This is the number of pixels at the camera. The m_{11} element of each pixel is collected in the upper corner and etc. for the other elements. In this way it is possible to construct the Mueller matrix of a large spatial area.

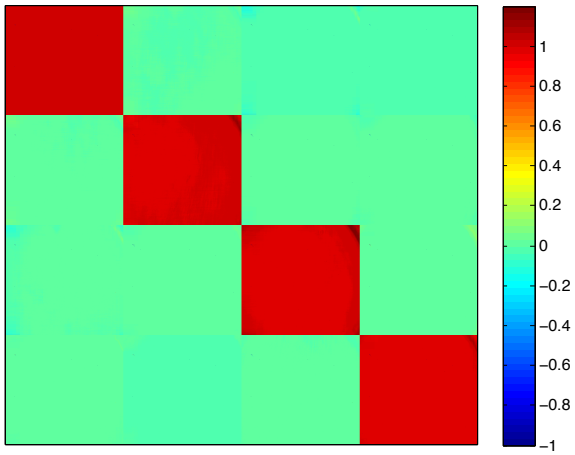

Figure 3: A good Mueller matrix of air given by the Mueller matrix ellipsometer. The matrix is close to be an identity matrix.

The Mueller matrix measurement of air in figure 3 have diagonalized elements close to one, while the other elements are close to zero. The same matrix is showed in figure 4 with different colorbar.

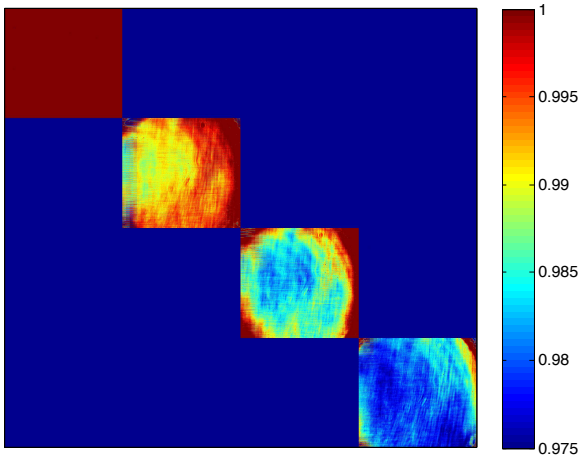

Figure 4: The matrix from figure 3 with different colorbar. The laser beam is clearly visible in the diagonal elements of the matrix.

The circles of the diagonal elements are the laser beam, which does not cover the elements in figure 4 in a smooth way. This makes the off center parts of the elements not trustworthy. It is better illustrated by another Mueller matrix of air, figure 5, where the outer parts of the elements are clearly not the identity matrix. The central area of the each Mueller matrix element is close to unity, but at the periphery the values are getting wrong. Taking several Mueller matrices could solve this problem, by overlapping in a way that only included the central part of the Mueller matrices.
Another use of the air sample is to reveal if something is wrong with the ellipsometer. The matrix in figure 6 shows this.
In figure 6 all the diagonal elements are to low. This problem was caused by improvements of the ellipsometer.

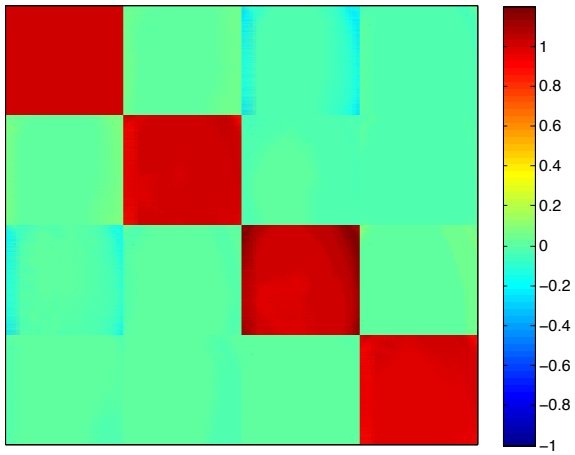

Figure 5: Another Mueller matrix of air given by the Mueller matrix ellipsometer. The central area of the each Mueller matrix element is close to the identity matrix, but at the off center the values are getting to low.

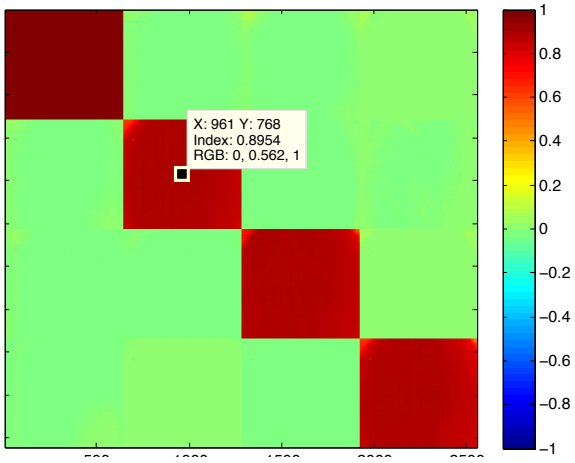

Figure 6: A bad Mueller matrix of air given by the Mueller matrix ellipsometer. The diagonalized elements are to low. The problem was caused by improvement of the ellipsometer.

6 Crystalline phases of liquid clay

Clays are silicates with layered structure. There are many versions of clay, but in this report the synthetic clay Na-fluorohectorite will be studied. Na-fluorohectorite is made of Li-fluorohectorite by ion-exchanging and will only be briefly discussed here. A more comprehensive study is given in Lindbo Hansen [14], which makes the basic of this section.

6.1 The layered structure

The layered structure of Na-fluorohectorite is illustrated in figure 7.

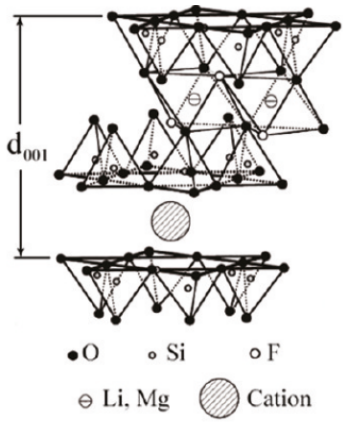

Figure 7: The layered structure Na-fluorohectorite where the cation is Na^+. d_{001} shows where the structure starts to repeat. Figure is from [15].

The layered structure of Na-fluorohectorite is called triocthahedral 2:1. When Na-fluorohectorite is dispersed in saline water the layers do not exfoliate, but keeps their lamellar structure. This is illustrated in figure 8.

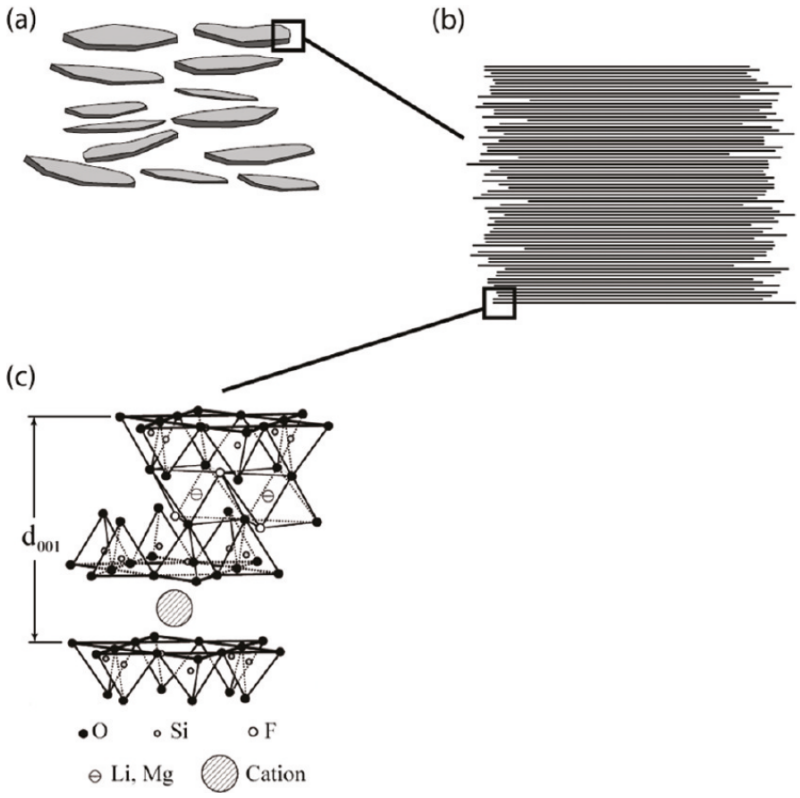

Figure 8: Na-fluorohectorite dispersed in saline water, where it forms lamellar particles illustrated by figure a). Each lamellar consists of several layers that are presented in b). Figure c) is the same as figure 7 and shows how the layers are constructed. Figure is from [15].

In this report Na-fluorohectorite will be described by looking at the lamellar particles, which can be considered the basic component of clay in aqueous dispersions. The way the lamellar particles interact with each other and its surroundings explain several of the properties of the dispersed clay.

6.2 The lamellar particle

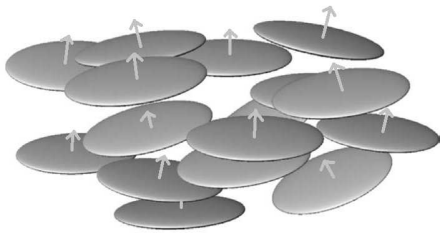

Figure 9: The "discs" illustrate the lamellar particles. The arrows are the optical axes of particles. The particles are organized as in a nematic phase, where the particles have directional, but no positional order. Figure is from [14].

The lamellar particle is illustrated in figure 9. The particles are polydisperse, meaning that the size of the particles varies. For Na-fluorohectorite the diameter of the "disc" is about 1 μm, while the thickness is from 10 to 150 nm, or about 20 to 100 layers. The arrows of figure 9 are the optical axes, showing the orientation of the particle. When Na-fluorohectorite is dispersed in a saline dispersion, lamellar clay particles will be dispersed and dominate much of the dispersion. The polydispersity of the lamellar particles will allow the gravitational force to sort out the particles by size in a process that will take from hours to weeks. The result is that the bottom of the dispersion will be dominated by debris and the biggest lamellar particles. Higher up the concentration and the size of the particles will fall. The entropy of the system will decide the direction of the optical axes. One could believe that a random orientation is preferred, but it has been proved that the interaction between the lamellar particles will sometimes give a preferred orientation. This give raise to the nematic phase, illustrated by figure 9, where the particles have directional, but no long range positional order.
Above the nematic phase one will find the smallest lamellar particles in a low concentration, which leads to an isotropic phase. The

optical axes of the particles are random and have no connections with the neighbors. At the top of the dispersion it will be formed a pure phase where there are no particles.

6.2.1 The anisotropy of lamellar particles

The lamellar particles can be described as an uniaxial material, illustrated by figure 10.

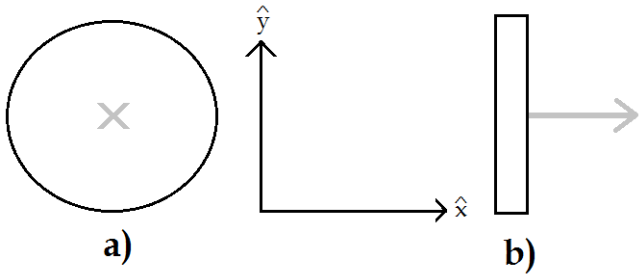

Figure 10: A lamellar particle viewed from different angles. In subfigure a) the particle is viewed at the front with the optical axis pointing out of the paper. Light linearly polarized along the x-axis will experience the same refractive index as y polarized light. In subfigure b) the lamellar particle is viewed from the side. x polarized light will experience a different refractive index than y polarized light.

Light traveling in the z-direction of figure 10 will experience the particles differently. The lamellar particle of subfigure 10a will be isotropic for the light, while the opposite is true for subfigure 10b. Here the x-axis will be the extraordinary axis and the y axis will be the ordinary one. If the particles are organized like subfigure 1, the anisotropic area will be felt as isotropic. The reason for this is that the light only sees the projection of the refractive index in the x-y plane. In the rest of the article, the projected smaller refractive index will be termed the fast axis, while the larger projected index will be the slow axis.

6.3 The nematic phase

The lamellar particles will experience two different forces between each other. One is the van der Waals attraction, while the other is the electrostatic Coulomb repulsion. The last force has its ori-

gin when Na-fluorohectorite is made of Li-fluorohectorite by ion-exchanging, causing the clay to have a charge distribution. Sometimes the charges are screened by electrolyte ions and the particles will behave as single particles, beyond that the optical axes tend to be in the same direction. Such a nematic phase is called nematic soil. If not enough electrolyte ions are available, the particles create extended networks known as nematic gels. Those networks is called tactoids.
Which direction the optical axes have in a nematic phase is random when the particles are not influenced by external factors like magnetic field or the walls of the container. It has been shown that near the walls of the container or at a phase transition a homeotropic alignment takes place, illustrated by figure 11.

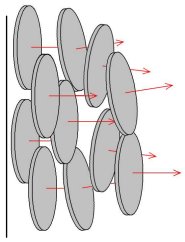

Figure 11: The homeotropic alignment of lamellar particles. The optical axes are perpendicular to the wall, represented by the black line. Figure is from [14].

7 Experimental setup

An interesting phenomenon to examine is how clay dispersed in water is behaving. By shaking clay and saline water to make a homogenous dispersion and using transparent capillaries to contain the mixture, it is possible to study how different phases appear and evolve. The Mueller Matrix Imaging ellipsometer is exceptionally well suited to perform this task. The result of such a study should reveal a considerable amount of information about the spatial variations of the structures of the different phases.

7.1 Preparations of samples

In this experiment two types of Na-fluorohectorite dispersions with three types of capillaries where used. The differences of the capillaries where just size, while the different Na-fluorohectorite dispersions had been prepared in different ways. The following subsubsections will explain the differences.

7.1.1 Capillaries

The capillaries will be in three different sizes: small, medium and large. The small has the inner dimensions of 0.2 mm · 2 mm · 50 mm, the medium is 0.4 mm · 4 mm · 50 mm and the large is 1 mm · 10 mm · 100 mm. The different capillaries can be viewed in figure 12:

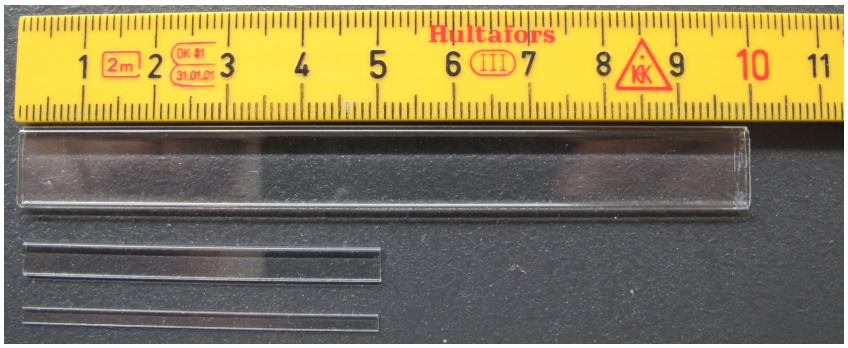

Figure 12: Large, medium and small capillary.

7.1.2 Uncentrifuged Na-fluorohectorite

This was the most basic of the dispersions. It was made of 5.52 gr 3mM NaCl saline water and 0.171 gr clay. The mixture was shaken by a mechanical shaker (Heidolph Vibramax 100) for two hours. The resulting opaque and homogenous dispersion was put into capillaries of different sizes.

7.1.3 Centrifuged Na-fluorohectorite

This dispersion was made of Na-fluorohectorite and 10^{-3} M NaCl water in proportion 0.500 gr clay to 30 mL water. The mixture was shaken by a mechanical shaker (Heidolph Vibramax 100) for an hour. Then it was ultrasonicated in one and a half hour in an Bransonic 5510 Ultrasonic Bath in order to dissolve unsolved clay. The mechanical shaker shook the resulting opaque dispersion another hour to ensure complete dissolution. Then the sample was centrifuged by a Jouan B4i centrifuge for one hour at 2000 rotation per minute. The largest particles were centrifuged at the bottom of the sample and only the isotropic phase above was extracted. The resulting relative clear sample was shaken yet another hour, before it was put into capillaries of each size. The centrifuged and uncentrifuged Na-fluorohectorite can be viewed in figure 13.

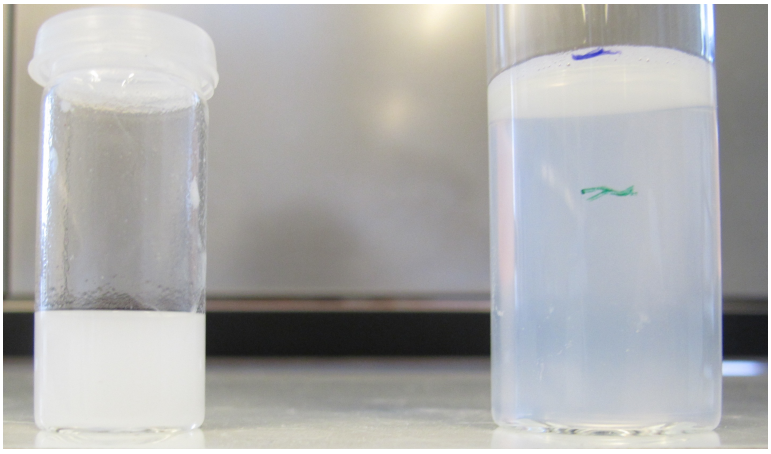

Figure 13: Uncentrifuged Na-fluorohectorite to the left and centrifuged Na-fluorohectorite to the right.

7.2 Problems of capillaries

A problem that should cause several setbacks in the experiments was how the capillaries was enclosed. The small and the medium was stopped up by melted wax that congealed at the ends of the capillaries. This turned out not be an optimal solution because the wax often did not seal of the ends completely. The result was leakage or air bubbles that destroyed the samples, often several days after the sample were made. There was similar problem with the film used to enclose the large capillary. The ruined samples had to be replaced, causing several delays. Luckily there was made enough dispersion in the start of the experiment to replace the losses. The old dispersion was simply shaken by the mechanical shaker some hours before a new sample was made.
Another problem with the large capillaries was that the vertical sides were bowed. This caused them to act as lenses, making the measurements at the sides a little diffuse.
Although there were some problems with the large capillaries, the small and medium caused much more trouble. The results from the smaller samples will be reported, but the results from the large sample will be emphasized in this thesis.

7.3 Mueller matrices of the different samples

At regular times the samples was studied by using the Mueller Matrix Ellipsometer. The sample was mounted on a stage that could be raised, lowered and rotated sideways mechanically. The stage can be viewed in figure 14, where the upper part of the sample is covered by the set up. Then multiple pictures were needed in order to get the intensity matrix, $\mathbf{B}$, of the whole sample. The Mueller matrix $\mathbf{M}$ was obtained by using the process described in section 5.1. Then the Mueller matrices were numerically stitched together in a way that discarded the outer parts of the Mueller matrix. This ensured that only the central and most trustworthy part of the Mueller matrix was used for analyzes and discussion.

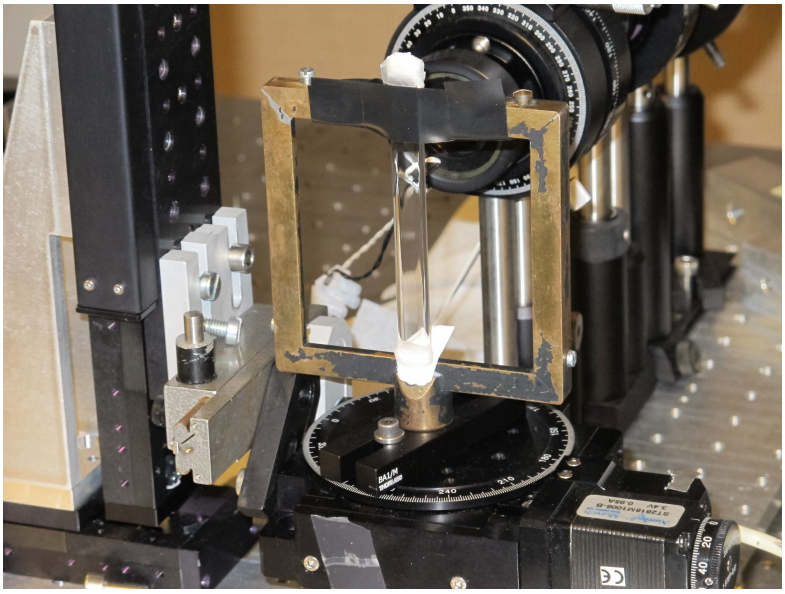

Figure 14: The stage that kept the samples during measurement. The sample could be rotated, elevated and moved sideways. In the background the PSA of the ellipsometer can be viewed.

8 Results and discussion

The Mueller matrices from each type of sample will be presented, analyzed and discussed in their own subsection. The presentation was a challenge because the interesting part was at the bottom of long capillaries. The Mueller matrices are not usually presented in their natural form, but the vertical axis have been scaled up relative to the horizontal one. In addition the upper part of the matrices have usually been cut off. The size of every Mueller matrix element will be given in the caption of the figure.
In the following subsubsection there will be analyzes and discussion. The analyzes will mainly rest on the degree and direction of the retardance, which are given by equation (22) and (23). The parameters will reveal the degree of anisotropy and the direction of the fast axis of lamellar particles in the anisotropic areas. As figure 10 illustrates one will only get a 2D map of the retardance, a projection in the x-y plane. When the particles are organized like figure 10a, the ellipsometer will not see the retardance, making anisotropic areas apparently isotropic. On the other hand, when the particles are organized like figure 10b the ellipsometer will see the whole retardance. Usually the particles will be organized somewhere in the middle, meaning that some of the retardance will be hidden. In addition the degree of depolarization will sometimes be discussed. Since $\mathbf{M_\Delta}$ of forward decomposition is not of the same form as equation 15), another definition of Δ has to be used [9]. The analyzes of the different Mueller matrices will rest on forward Mueller matrix decomposition. The MATLAB code used to obtain the decomposition, the retardance and the other parameters have been written by the PhD-students Lars Martin Sandvik Aas, Pål Gunnar Ellingsen and Frantz Stabo-Eeg. Their works where based upon the articles of Lu and Chipman [3] and Manhas et. al. [5].
In order to present the direction of the fast axis, a color map from -90° to 90° will be used. The direction of the fast axis is given in figure 1. -90° means that the optical axes are pointing straight to the left, 0° means that they are pointing right up, while 90° means that the optical axes are pointing straight to the right. A rotation of the lamellar particle by 180° gives no difference, so -90° is the same as 90°.
When the retardance and depolarization is presented, the vertical

axis will give the distance to the top of the sample. As discussed in section 7.3, the stage did cut of the top of the sample, so the vertical axis will start at a higher number than zero.

8.1 Centrifuged clay, large sample

8.1.1 Results

The Mueller matrices of the samples are presented in figure 15-19. Two large samples of centrifuged clay were made, called C1 and C2. Because the action always happened at the lower part of a long sample, it was necessary to skip the upper part and scale up the horizontal axis relative to the vertical one. The only exception is figure 15, where no changes have been made. A survey of the different figures can be found table in 2.

Table 2: Survey of Mueller matrices for centrifuged samples.

Figures	Sample	Age and rotation of sample
15	C1	2 hours (0°)and 1 day (0°, 30 ° and 45 °)
16	C1	1 day (0°, 30 ° and 45 °)
17	C1	2 days (0°) and 4 days (0° and 45 °)
18	C1	14 day (0°, 45 ° and -45 °)
19	C2	4 days (0°), 14 days (0°) and 18 days (0°)

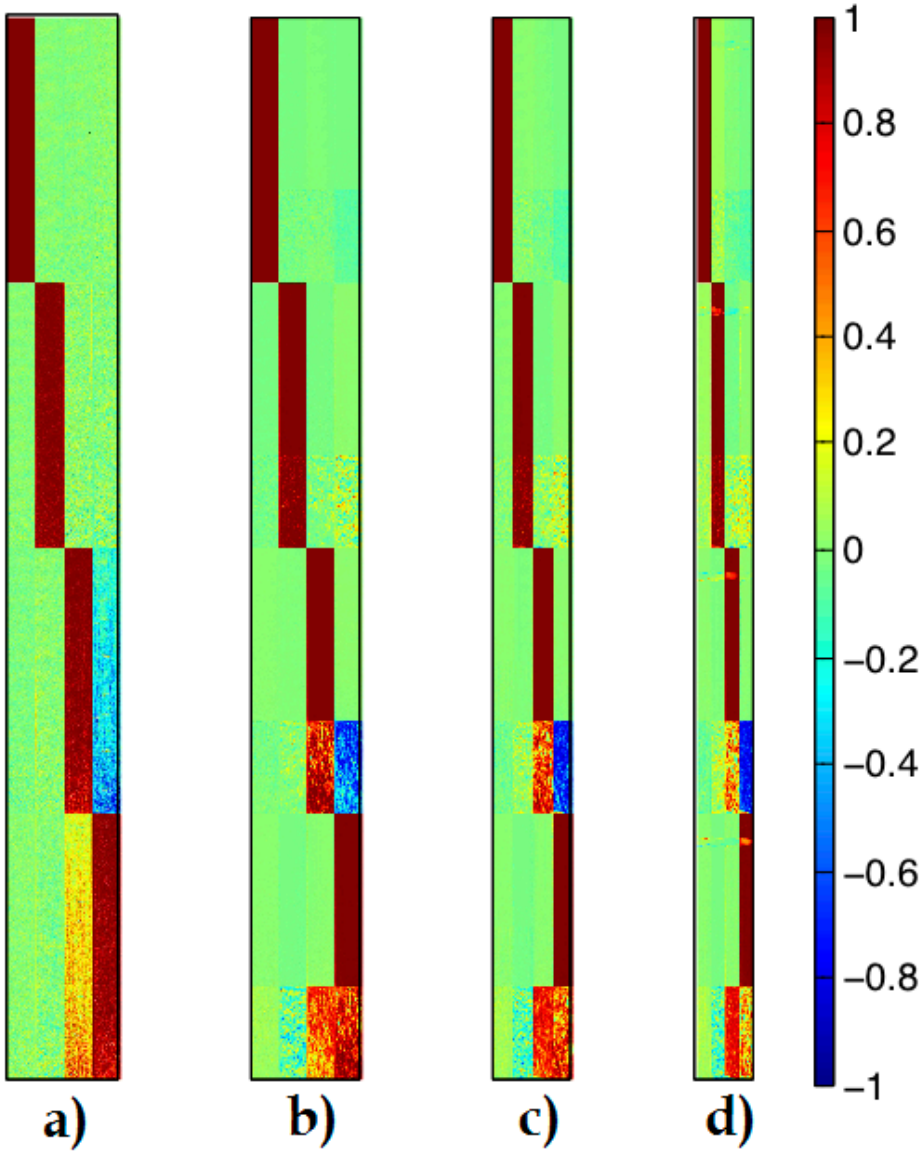

Figure 15: Mueller matrices of the large centrifuged sample. Each Mueller matrix element is 7.5 cm high and 1 cm wide. Subfigure a) is from about 2 hours after the sample was made. Subfigure b), c) and d) is one day old, but in subfigure c) and d) the sample has been rotated 30° and 45° respectively around the vertical capillary axis. The figure shows the creation of an anisotropic phase after 1 day that does not change by rotating.

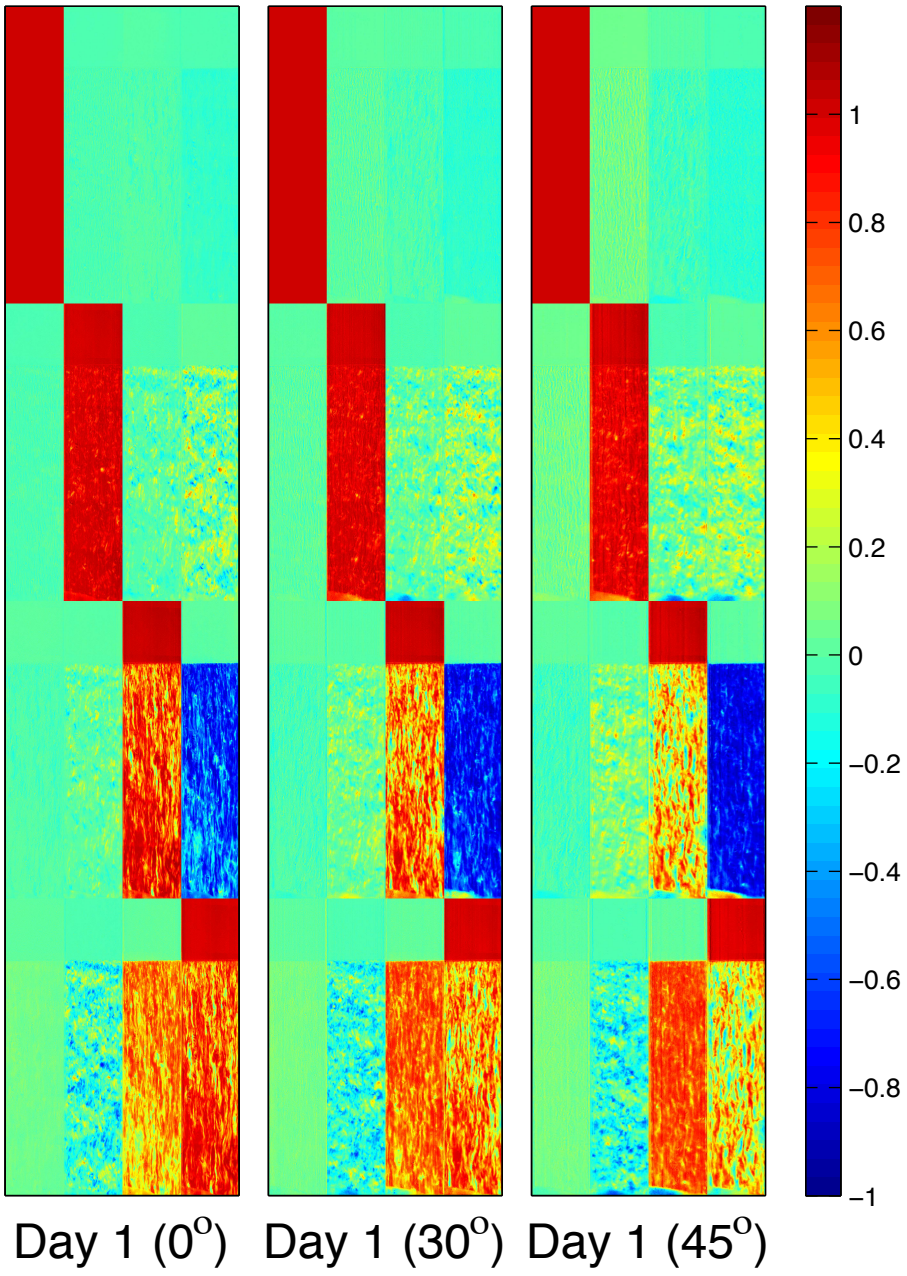

Figure 16: The bottom 3.33 cm of Mueller subfigure 15b), 15c) and 15d). Rotation of the sample is given in parenthesis. For better view the horizontal axis has been scaled up relative to the vertical.

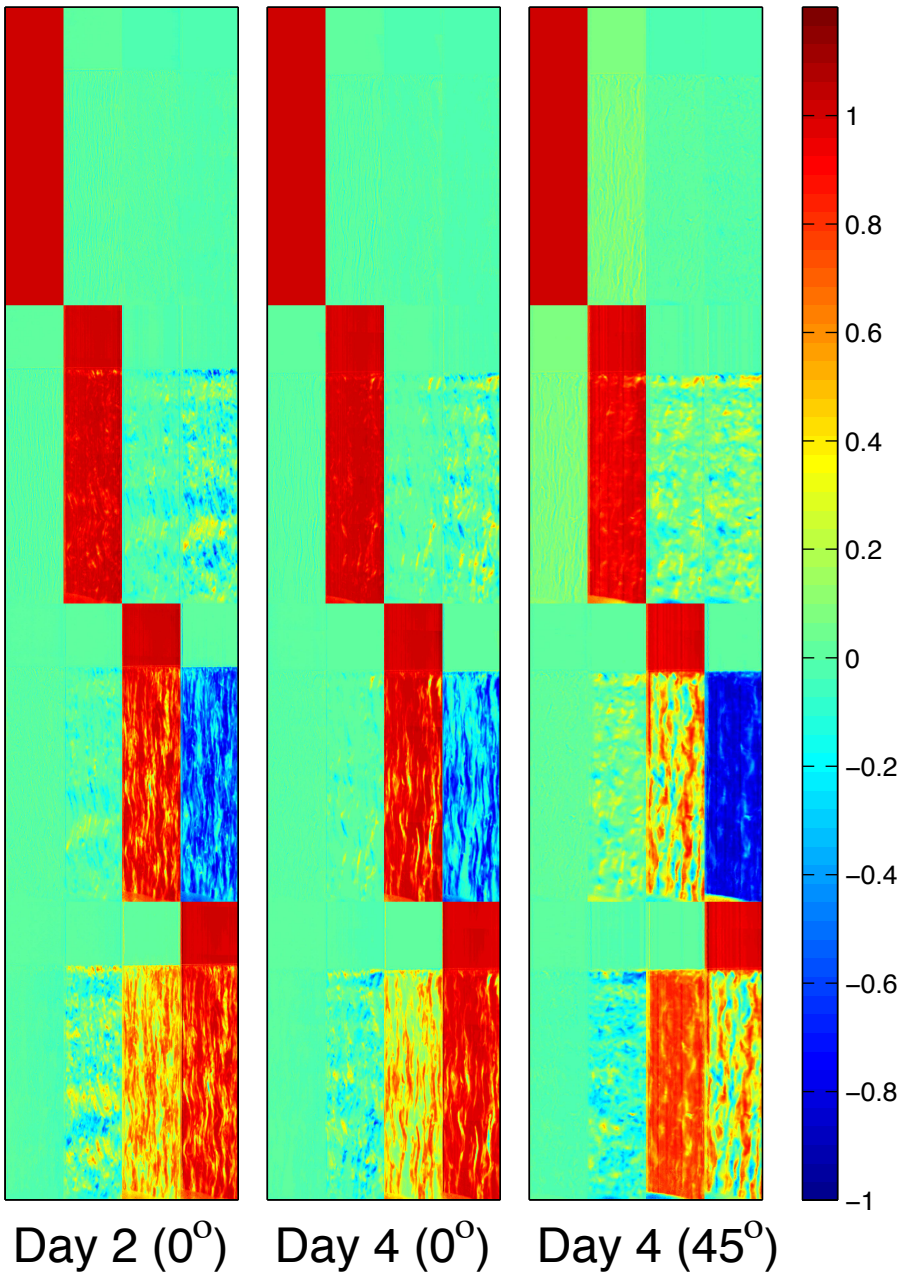

Figure 17: More Mueller matrices of the bottom 3.33 cm of the large centrifuged sample. Rotation of the sample is given in parenthesis. For better view the horizontal axis has been scaled up relative to the vertical. The off diagonal elements of the unrotated sample are fading, while the same is not true about the rotated sample.

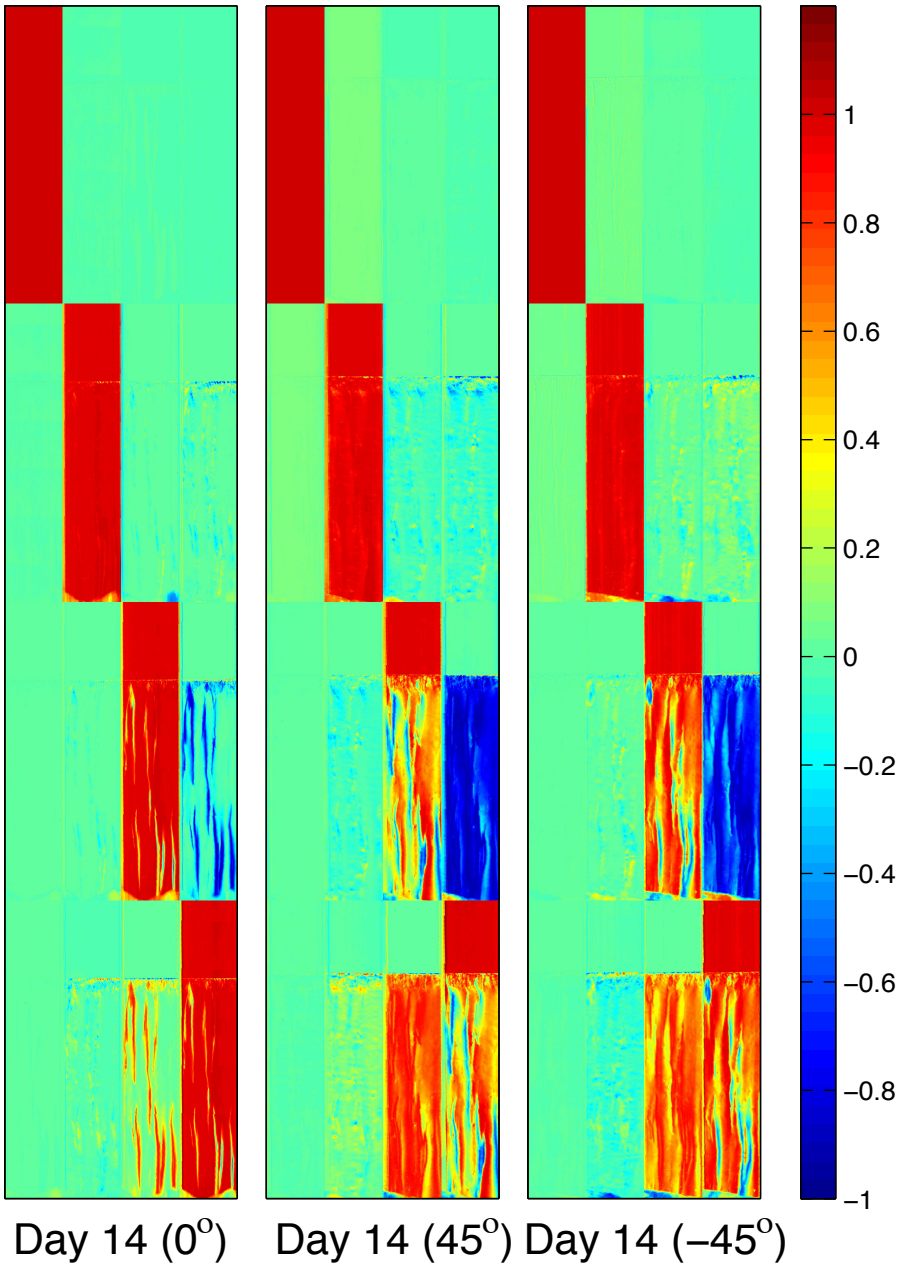

Figure 18: More Mueller matrices of the bottom 3.33 cm of the large centrifuged sample. Rotation of the sample is given in parenthesis. For better view the horizontal axis has been scaled up relative to the vertical. The matrix of the unrotated sample is close to resembling a pure transition matrix, while the matrices of the rotated sample have not changed much from figure 17.

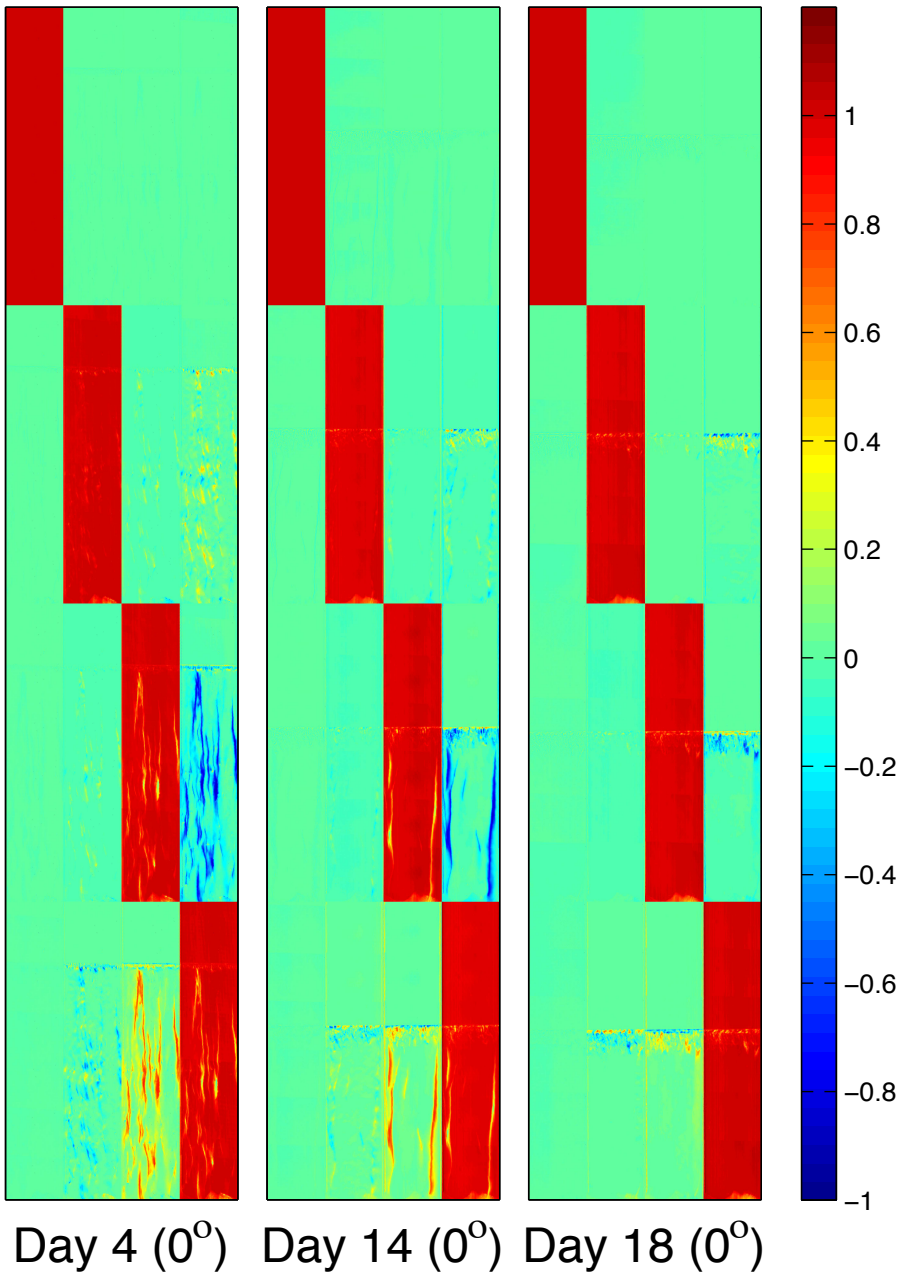

Figure 19: The Mueller matrices are from a physical different sample than the sample in figure 15-18. All the samples are unrotated. For better view the horizontal axis has been scaled up relative to the vertical. The Mueller matrix of the sample is resembling more and more a transition matrix, except at the phase border.

8.1.2 Analyzes and discussion

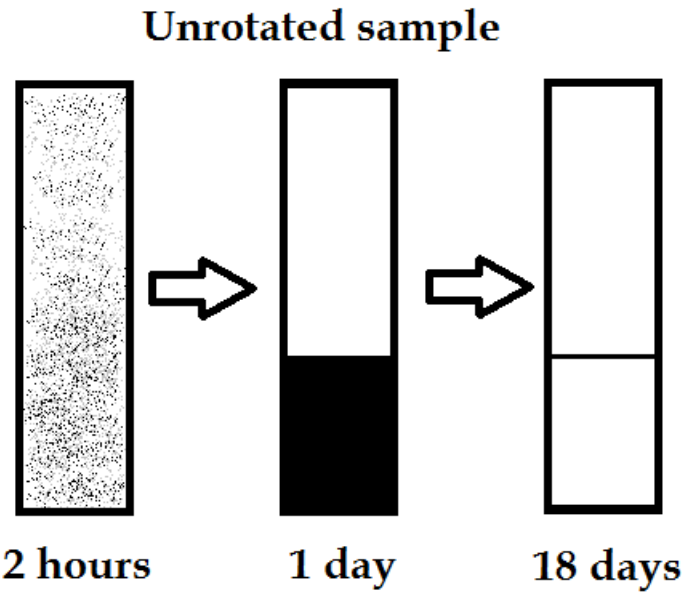

Figure 20: The development of a centrifuged unrotated large sample, based on the figures 15-19. Dark areas mean high degree of projected anisotropy, while white areas mean low. After one day the sample has developed two phases, the upper one has low projected anisotropy and the lower one has high projected anisotropy. After 18 days the projected anisotropy of the lower phase has disappeared except at the phase border.

The main development of the centrifuged sample can be seen in figure 20 and 21. First the dispersion is relative homogenous, but after one day an isotropic and an anisotropic phase have appeared. The anisotropic phase of the rotated sample is stable, while the anisotropic phase of the unrotated sample seemingly has disappeared at day 18. Only a tiny stripe between the two phases has kept its anisotropy. In order to understand the development it is necessary to use the forward decomposition and analyzes tool described at the beginning of this section. In figure 22 the result of the forward decomposition of the first matrix from figure 17 is presented. The figure shows that the focus of further examination should be retardance. $\mathbf{M_D}$ is close to the pure transition matrix, while $\mathbf{M_\Delta}$ has some, but not many, deviations from a transition matrix. This

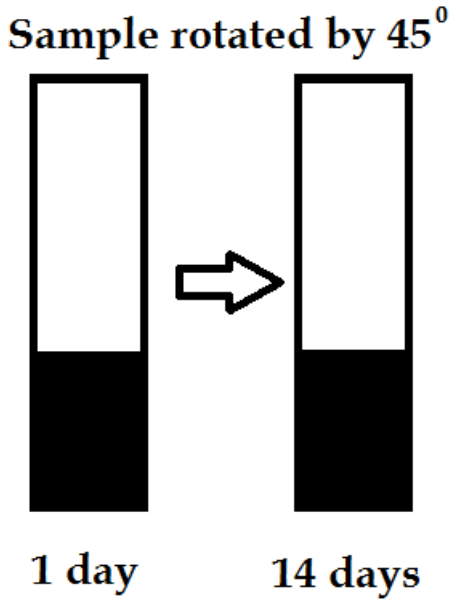

Figure 21: The development of a centrifuged large sample rotated 45°, based on the figures 16, 17 and 19. Dark areas mean high degree of projected anisotropy, while white areas mean low. The phases are stable.

is good, because it proves that there were little multiple scatterings. By looking at the retardance and the direction of the fast axis one should be able to determine the orientation of the lamellar particles in the anisotropic areas of the sample.
The first task is to study the tactoids and their corresponding stripes by looking at the retardance of the 2 hour old sample. The retardance and the direction of the fast axis are given in figure 23, where the middle echelons of subfigure 23a) are dominated by vertical stripes. This is the result of tactoids that have formed in the upper echelon and sunk [21], because of heavier density than the surroundings. The horizontal discontinuities of 23a) may be the result of that much happened in the first hours of the sample. A measurement took about 4 minutes and this was probably a too long timespan. The subfigure 23b) shows no corresponding stripes, maybe the movement of the tactoids smoothed away the pattern.
The next step is to look at how the anisotropic phase evolves the first days. In figure 24 the development of the degree of retardance

can be viewed from day one to day four for the C1 sample rotated by 0° and 45°. In figure 25 the corresponding changes of the direction of the retardance can be viewed.
The figure shows that the direction of the retardance is closing in to 90° for both rotated and unrotated samples over the same time span. In order to understand the result one has to remember that only the projection of the direction in the x-y plane is recorded. The lamellar particles are probably just tilted a little bit horizontal from their homeotropic alignment.
The fading process of the retardance of an unrotated sample is largely completed in figure 18. The retardance and the direction of the fast axis are showed in 26 and 27, where the C1 sample is rotated by 0° and 45°.
The figures confirm that the lamellar particles obtain a homeotropic alignment. This causes the projected retardance to largely disappear in an unrotated sample, but survives in a rotated sample.
The reason to this contradiction between the amount of projected retardance in an unrotated and rotated old sample is that the lamellar particles of the anisotropic phase starts to obtain a homeotropic alignment, illustrated in figure 11. The incoming laser beam only sees circles when it encounters the lamellar particles, so the result is that the anisotropic phase looks like it is isotropic.
The Mueller matrices from C2, given in figure 19, confirm this assumption. C2 had the same development the first days, but the measurements from day 4 shows that the off diagonal elements start to fade faster than the corresponding matrix of sample C1. At day 14 only vertical stripes of anisotropy have survived together with the anisotropy of the phase border. After 18 days the only anisotropic area of the sample is at the phaseshift.
The reason to why C2 started to fade earlier than C1 is not clear. One possibility is that the measurements C1 happened in a quiet time so it could be left in the stage between the measurements. The measurements of C2 happened at a much more busy time, so the sample had to be dismounted after every measurement. Although great care was taken in order not to stir up the dispersion some shaking and thrusting was inevitable. This may have helped to destroy the tactoids and made the transition to homeotropic alignment easier for the particles. That the phaseshift have moved down may be caused by the lamellar particles occupying less space when they

attain a homeotropic alignment. There are no matrices from a rotated C2.
Figure 28 shows the border between the phases. The direction of the retardance is close to 0°, meaning that the optical axes of the lamellar particles are pointing in the vertical direction. This is exactly what one should expect from an homeotropic alignment at the phase border [20].

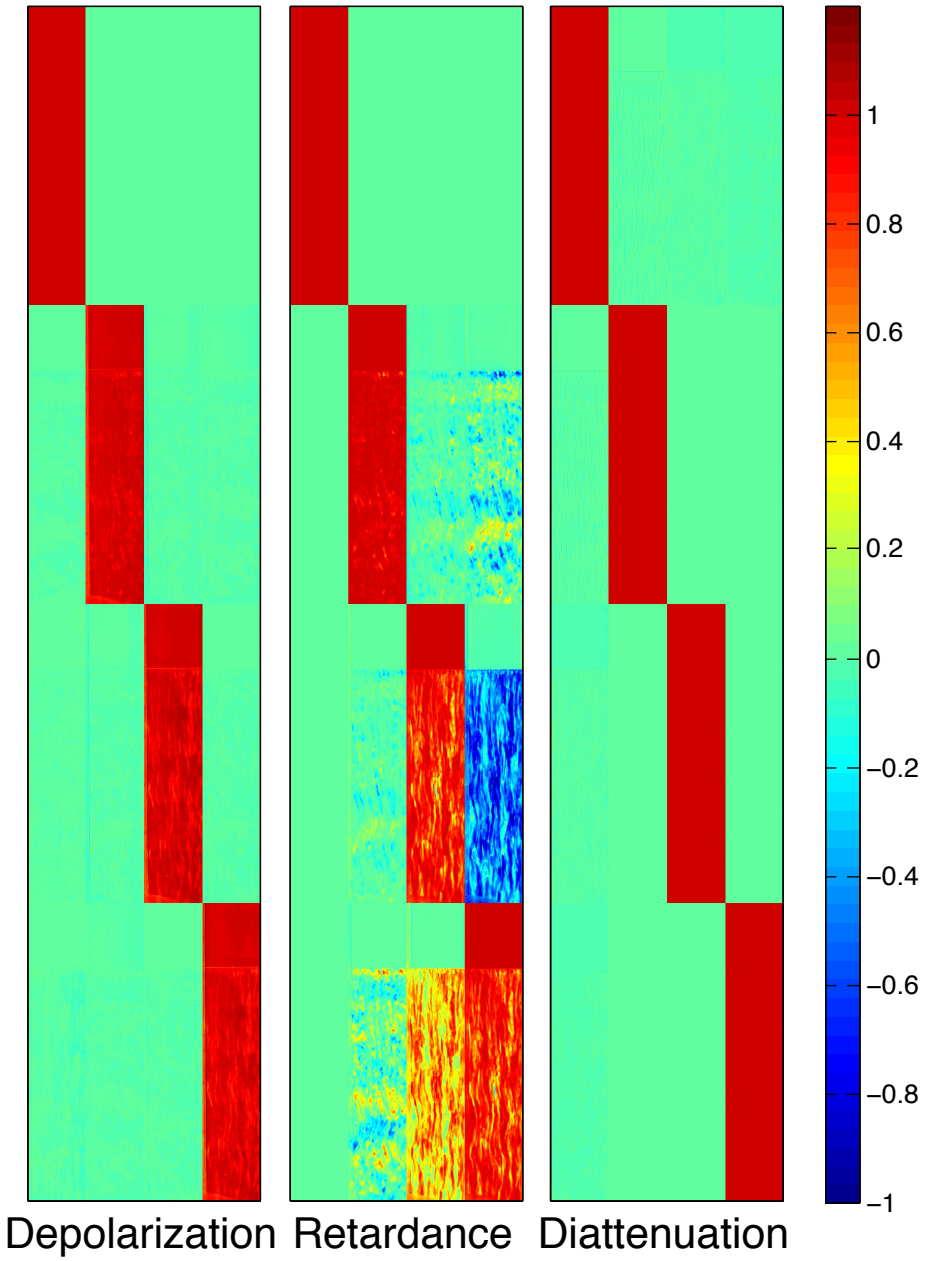

Figure 22: The result of a forward decomposition of the first matrix of figure 17. The depolarization matrix, $\mathbf{M_\Delta}$, retardance matrix, $\mathbf{M_R}$ and the diattenuation matrix, $\mathbf{M_D}$. $\mathbf{M_\Delta}$ and $\mathbf{M_D}$ is close to the identity matrix, while $\mathbf{M_R}$ is not.

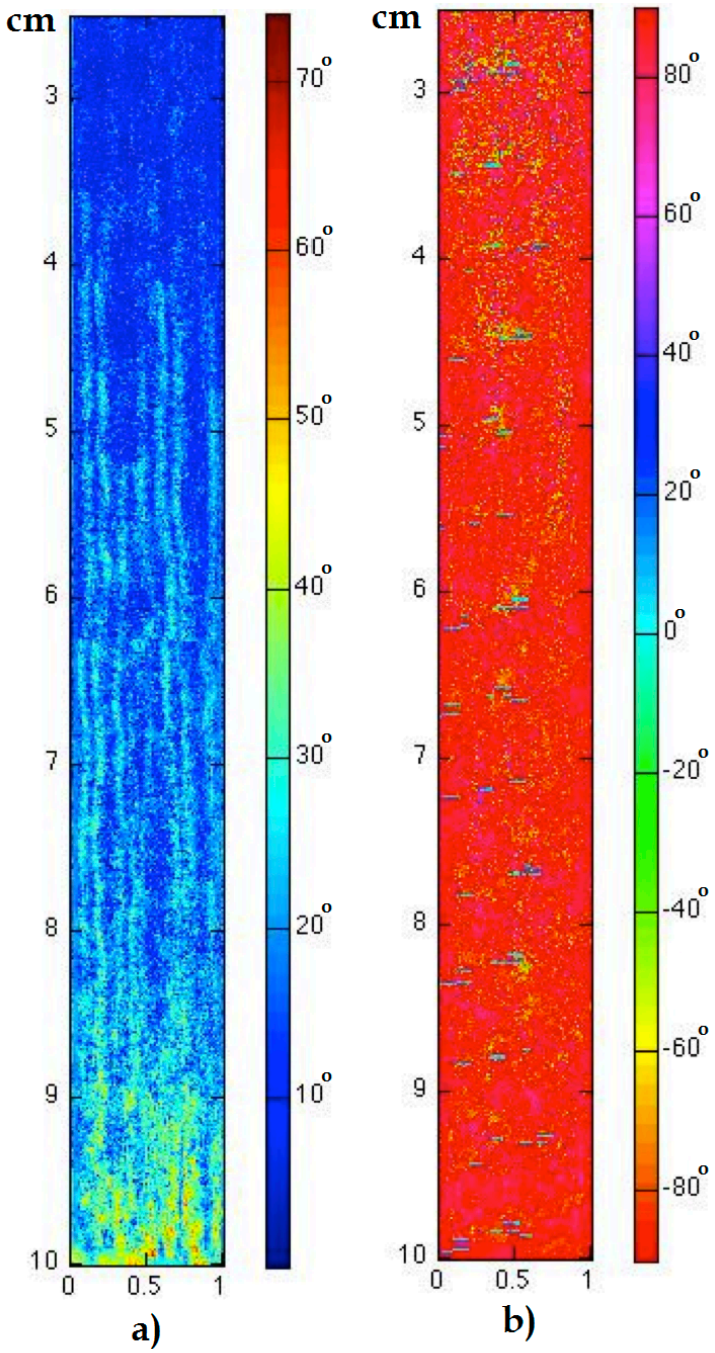

Figure 23: Subfigure a) shows the degree of retardance, while subfigure b) shows the direction of the fast axis. Both subfigures are from a two hour old unrotated sample. Notice the vertical stripes of subfigure 1.

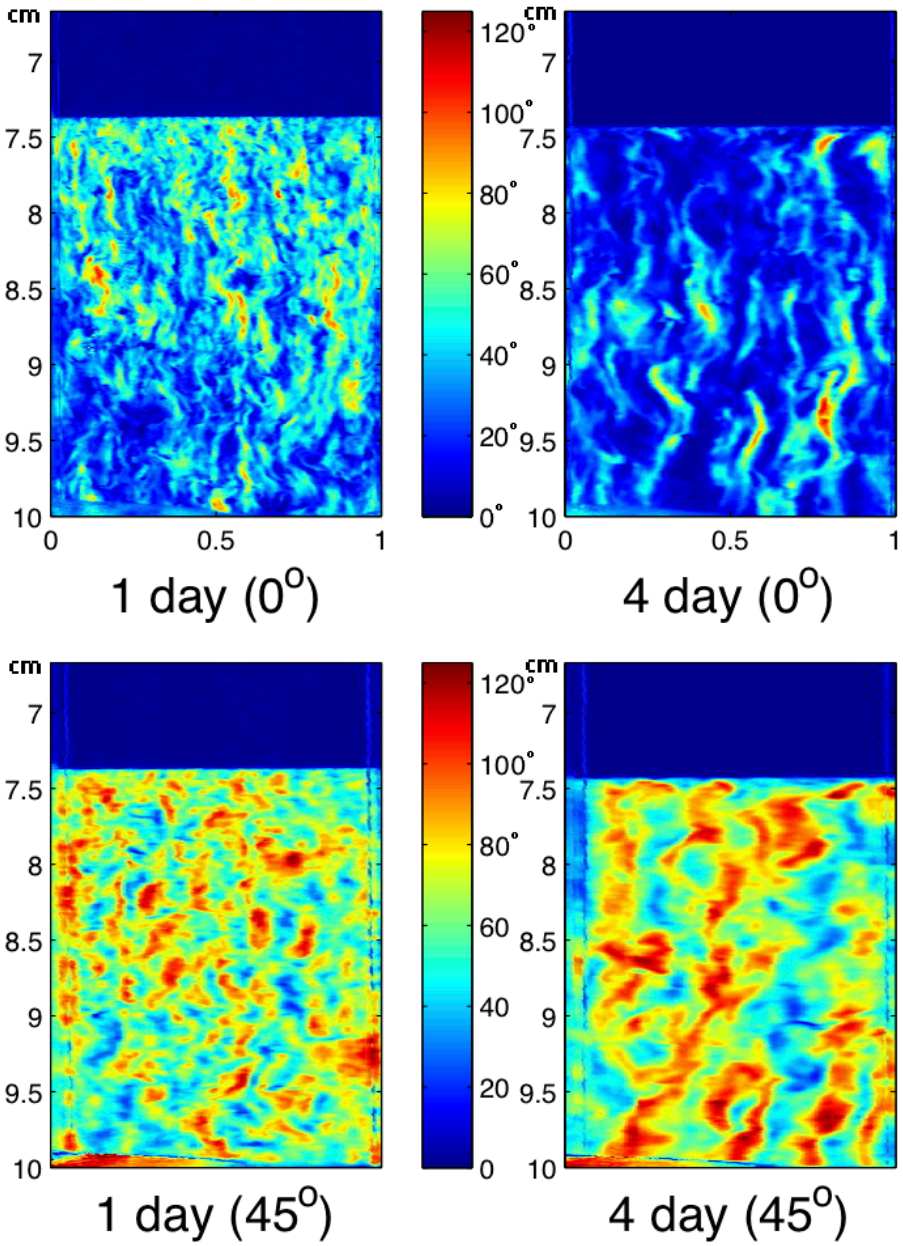

Figure 24: The subfigures show the degree of retardance for the bottom 3.33 cm of the large centrifuged sample at different ages and angles. Rotation by the sample is given in parenthesis. The notice that the retardance of the unrotated sample is vanishing, while the retardance of the rotated one stands firm. The units on the colorbar is degrees.

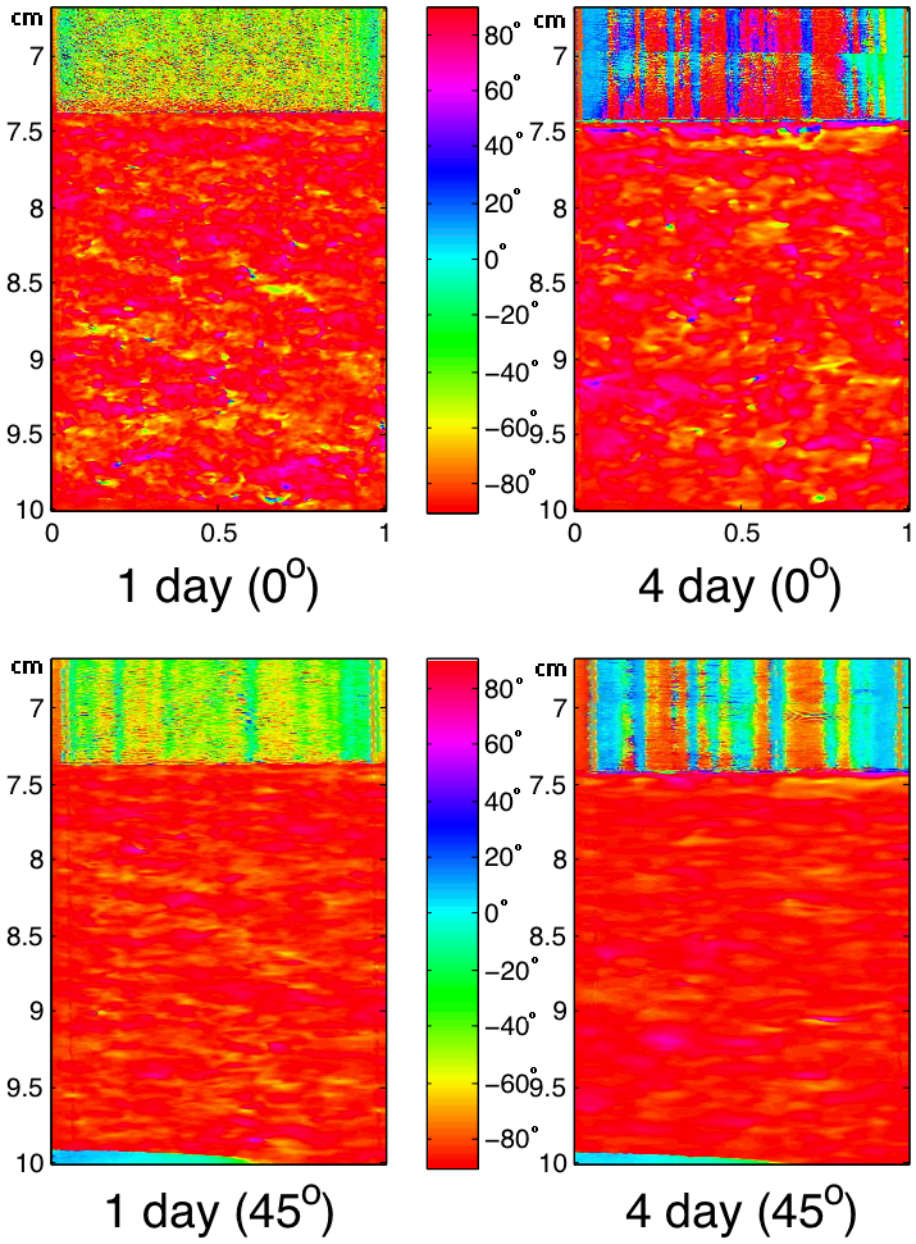

Figure 25: The subfigures show the direction of the fast axis for the bottom 3.33 cm of a large centrifuged sample at different ages and angles. Rotation by the sample is given in parenthesis. The units at the colorbars are degrees and straight up are 0°.

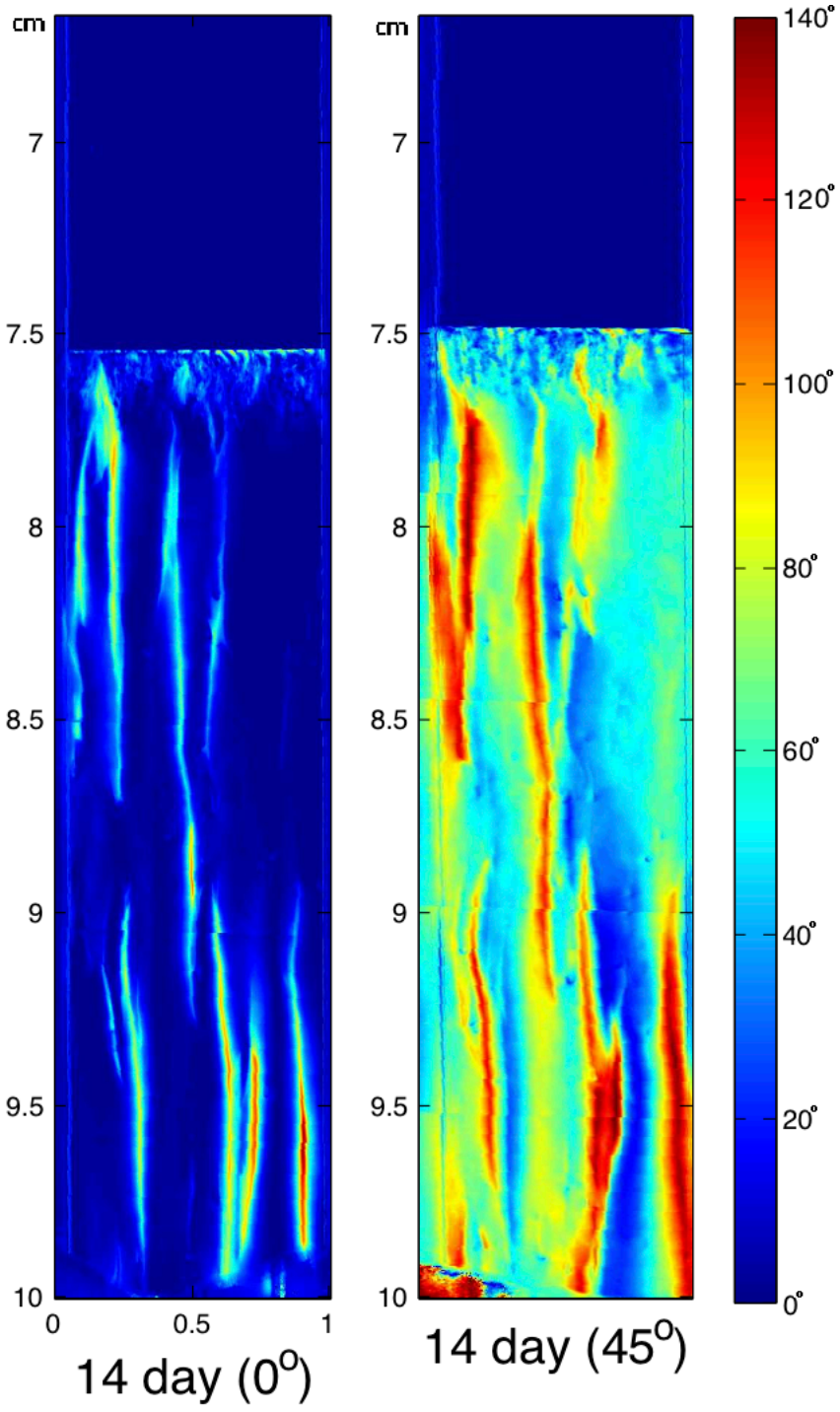

Figure 26: The subfigures show the degree of retardance for the bottom 3.33 cm of a large centrifuged sample. The projected retardance of the unrotated sample has disappeared, while it stands firm in the rotated one. The units at the colorbars is degrees

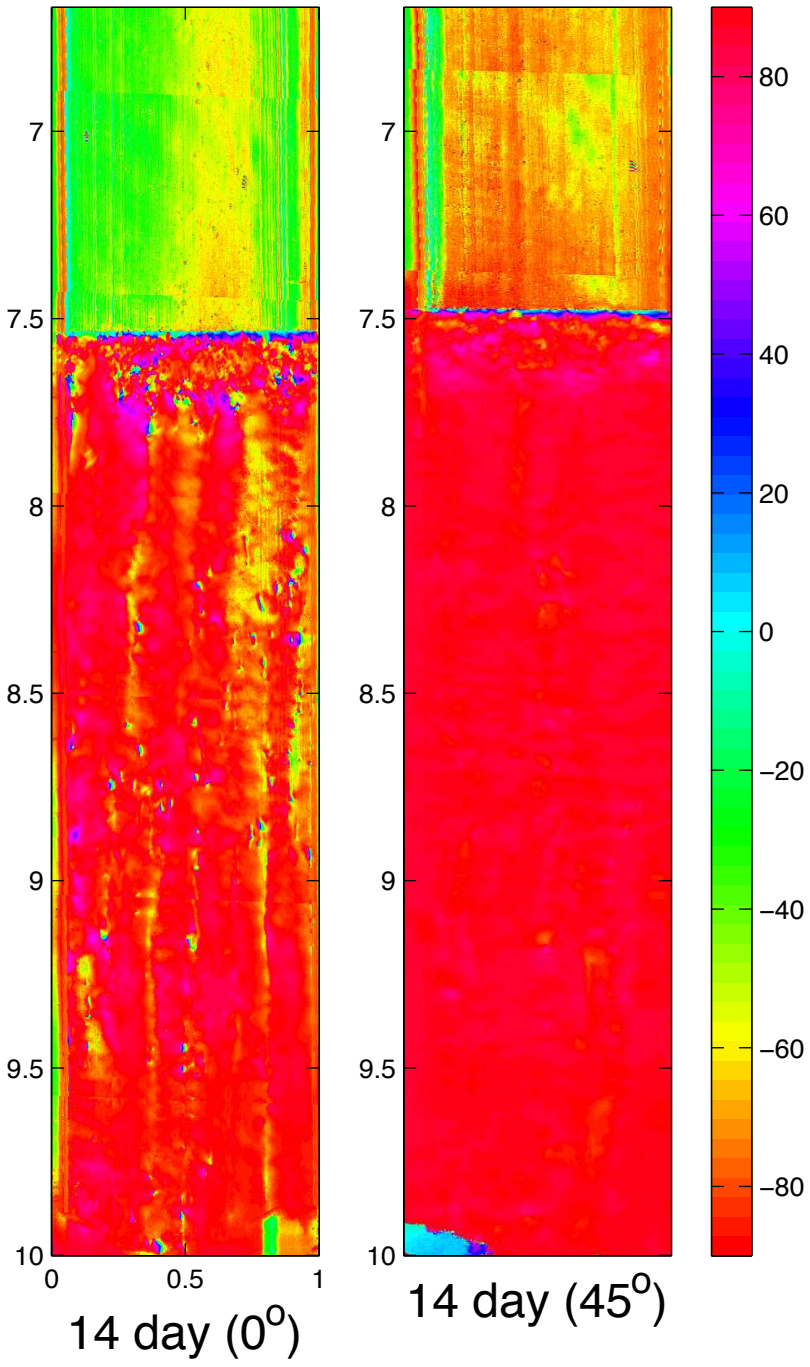

Figure 27: The subfigures show the direction of retardance for the bottom 3.33 cm of a large centrifuged sample. The units at the colorbars is degrees and straight up are 0°.

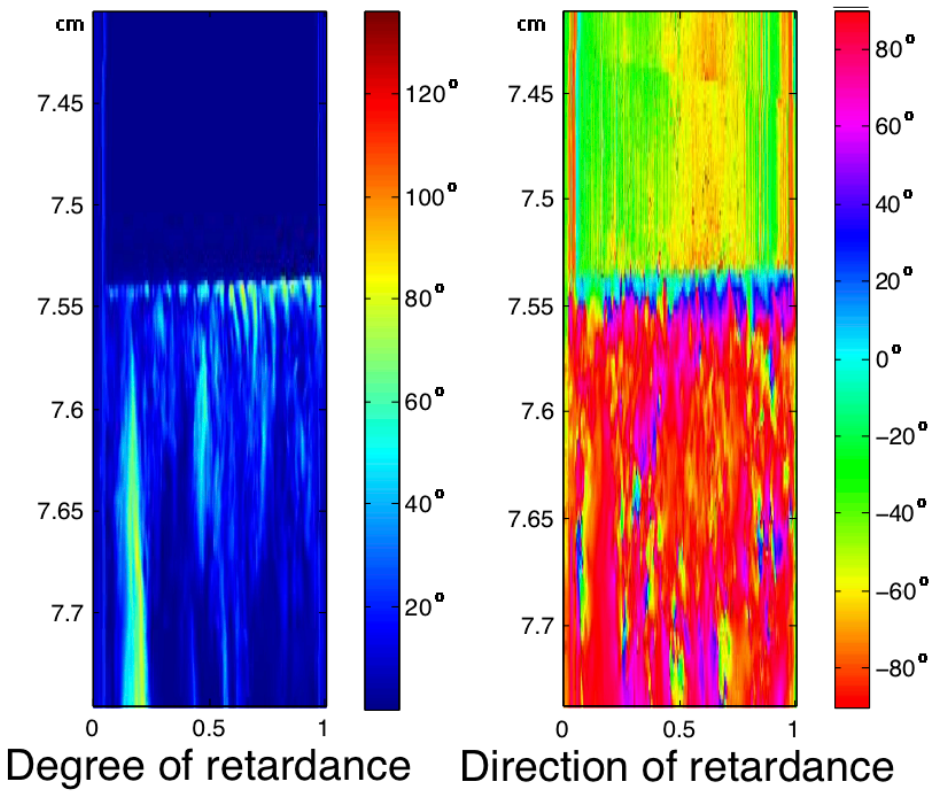

Figure 28: The direction and degree of retardance at the border between the anisotropic and isotropic phase. The figures are from the 14 days old unrotated sample presented in figure 26 and 27.

8.2 Uncentrifuged clay, large sample

The Mueller matrices of the uncentrifuged sample are presented in figure 29 and 30. The presentation of this type of sample will be in the same manner as the presentation of the centrifuged samples, although there will be no rotated samples. It was necessary to make two samples, U1 and U2, in order to cover the whole lifespan. The matrices from in figure 29 are from sample U1, while the figure 30 are from sample U2.

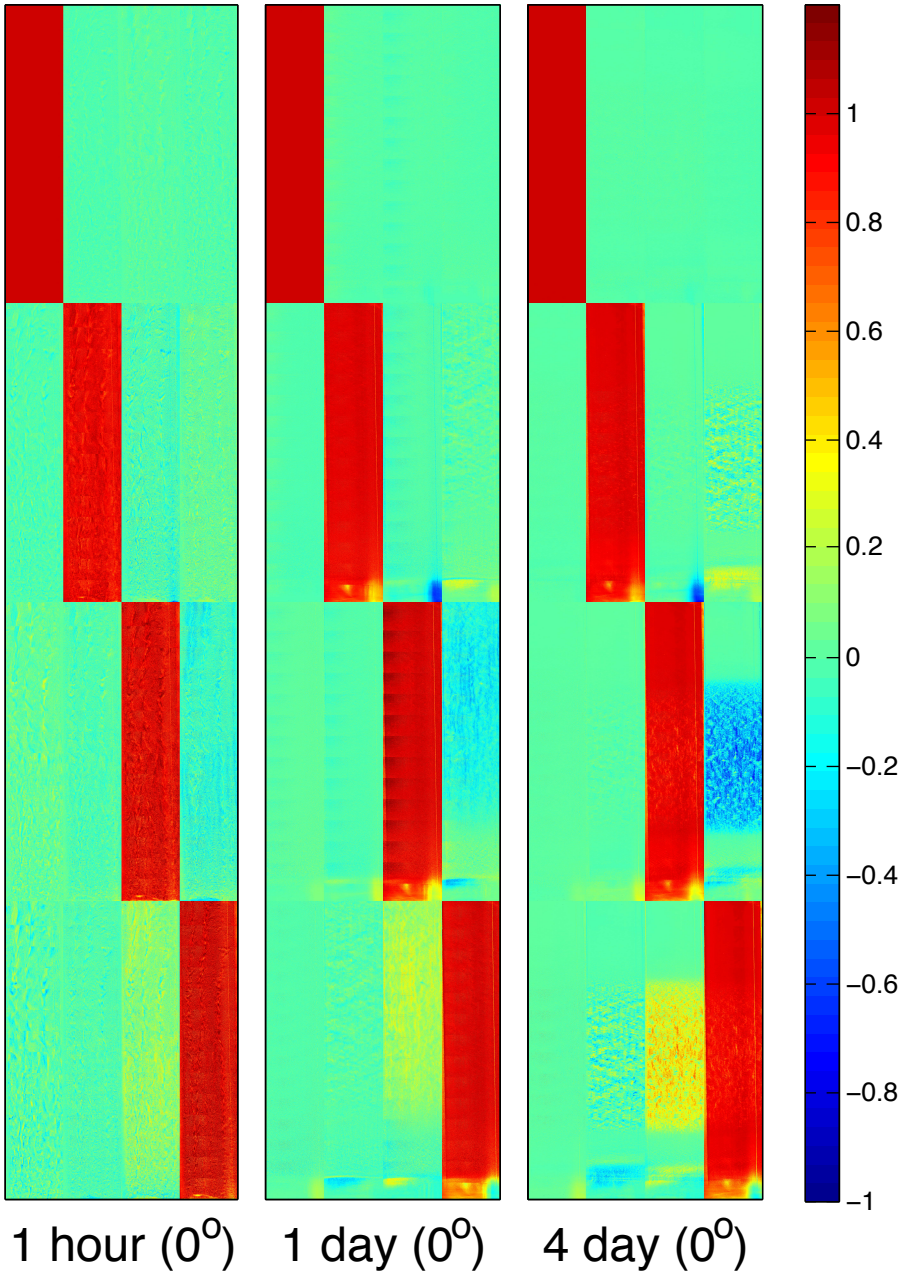

Figure 29: Mueller matrices of the bottom 7.5 cm of large unrotated uncentrifuged sample. In reality the Mueller elements are 1 cm wide and 7.5 cm high.

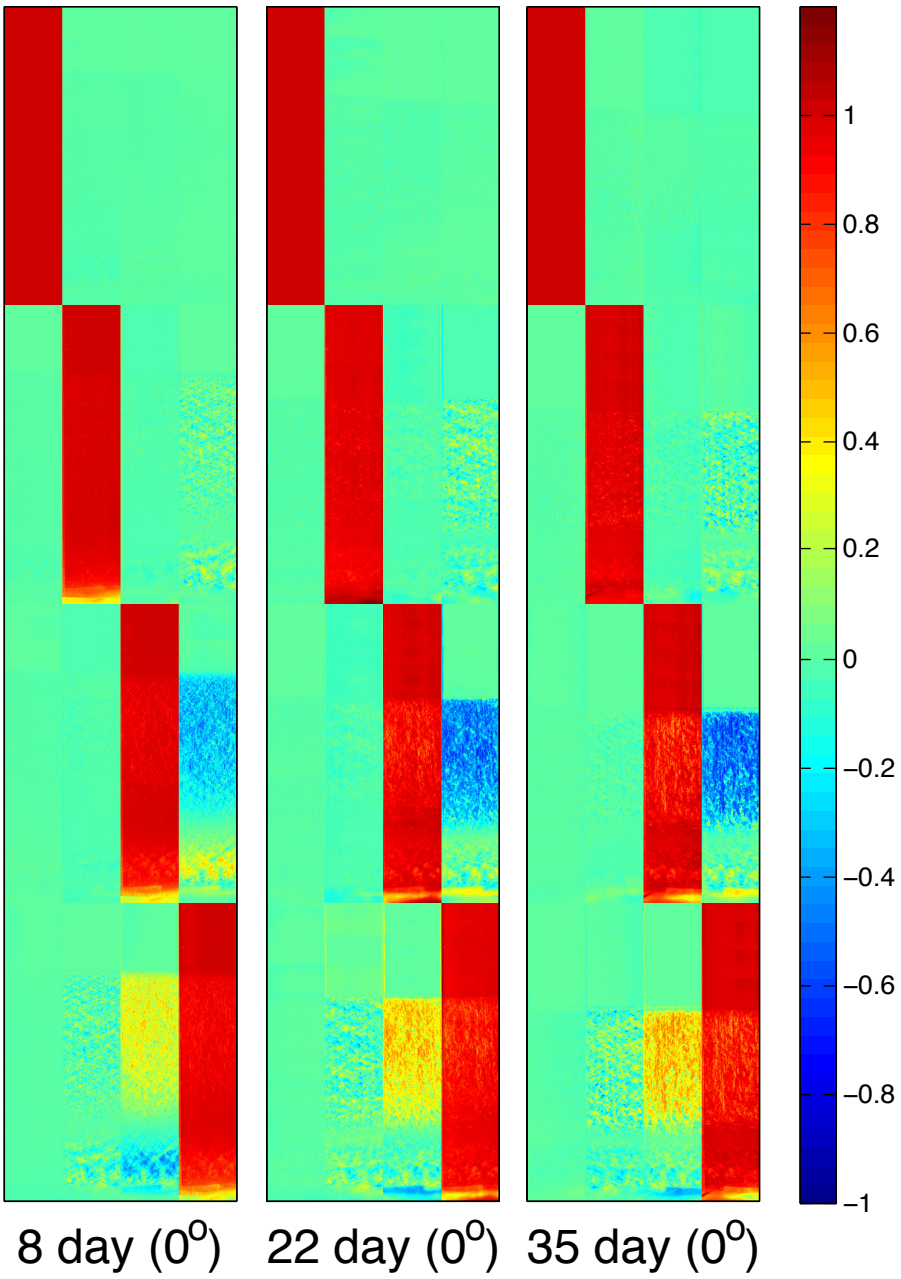

Figure 30: Mueller matrices of the bottom 5 cm large uncentrifuged unrotated sample. The Mueller matrices are from a physical different sample than the sample in figure 29. For better view the horizontal axis has been scaled up relative to the vertical axis. In reality the Mueller elements are 1 cm wide and 5 cm high.

8.2.1 Results

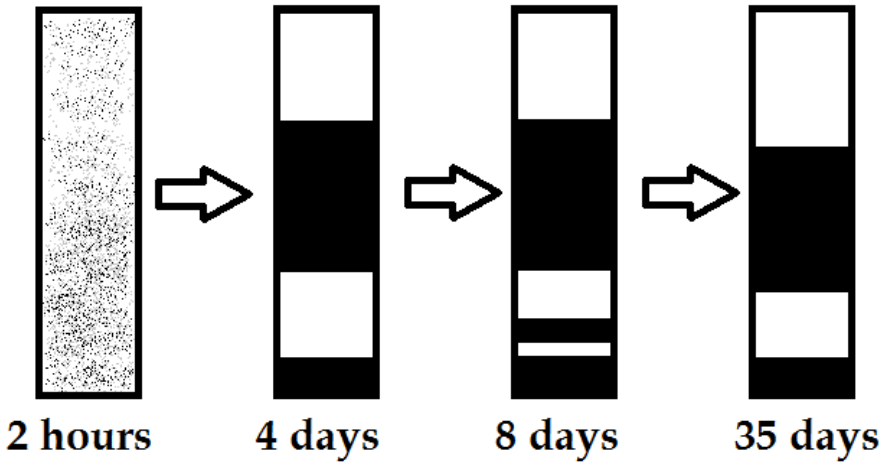

Figure 31: The development of the uncentrifuged large sample, based on figure 29 and 30. The dark areas mean high degree of projected anisotropy, while the white areas means low. After one day the sample has developed 2 phases with high projected anisotropy. There is a nematic phase in the middle of the sample, while the bottom has been sedimented. Both phases are stable, except that the nematic is moving down a little bit. In addition there is an anisotropic phase above the sediment layer after 8 days. Later this phase has disappeared.

The development of the large uncentrifuged sample is summarized by figure 31. After one hour the dispersion is relative homogenous, while at day 1 there is a nematic phase in the middle of the sample and the sediments have made a phase at the bottom. Both phases are stable, except that the nematic is moving down a little. In addition there is a anisotropic phase above the sediment layer after 8 days. Later this phase disappears.
The analyzes by using forward decomposition is more challenging in this case because of higher degree of depolarization. Multiple scattering is bad in itself and it gets worse because matrices are not commutative. The result may be that the matrices are wrong, as discussed in section 3.4.5. The extension and development of depolarization is illustrated by figure 32, where the degree of polarization is falling in the first period of the sample. This fall is probably caused by the creation of the sediment layer that drains the upper echelons for particles. In the last two subfigures the depolarization rise again.

The development of the degree and direction of the retardance is given in figure 33 and 34 respectively. The development of the degree of the projected retardance reflects the development of the depolarization. From 1 hour to day 8 the retardance fall, but it has risen again in at day 22 and 35. The orientation of the lamellar particles seems only to be locally, not globally, ordered in the anisotropic area of the sample. This may be a rest of the tactoids that was formed during the initial phase of the sample [21], meaning that they were locked in a configuration before equilibrium was obtained. Because of heavier density than the surroundings, the tactoids sunk in the sample and formed the anisotropic phase, where they were able to keep their initial orientation. Something seems to prevent a homeotropic alignment of the particles. It could either be the density or the size of the particles. The raise of depolarization and retardance in the late period may be the result of the contraction of the anisotropic phase, which causes heavier density of the lamellar particles.

The creation and disappearing of the anisotropic phase right above the sedimentary phase in figure 33 needs some attention. Lamellar particles may obtain a homeotropic alignment with the phase border to the sediments. This assumption is strengthened by figure 34, where the direction of the fast axis is showed. The corresponding area shows that the direction of the lamellar particles is pointing up. This should be expected from a homeotropic alignment. The reason to why the anisotropic phase diminishes is not clear. Maybe particles and tactoids falling from higher echelon destroy the alignments.

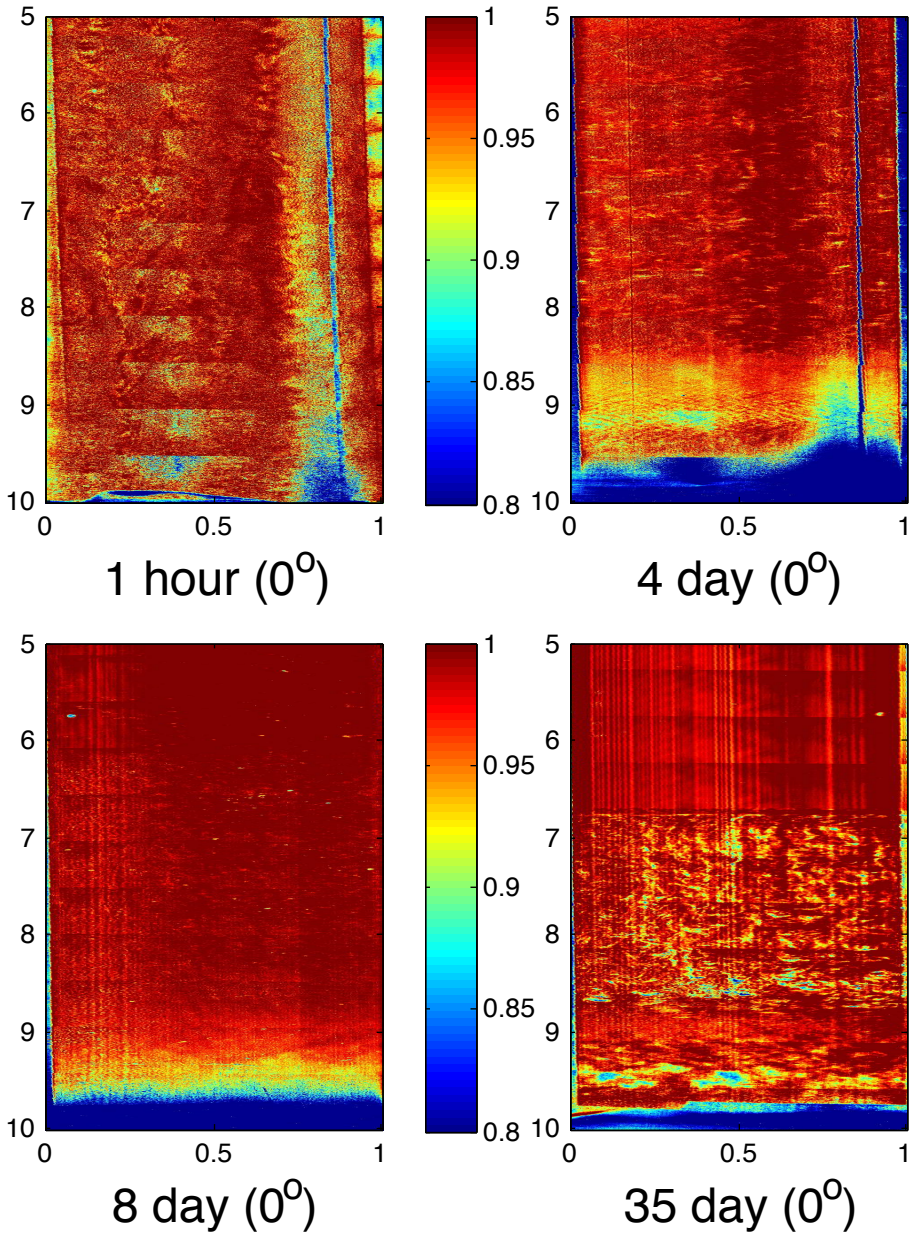

Figure 32: The degree of depolarization at the bottom 5 cm of uncentrifuged samples found by forward decomposition. 1 is no depolarization, while 0.8 is much depolarization. Notice that some of the depolarization is artifacts from the glass container, among other the depolarization from the isotropic layer in the last subfigure.

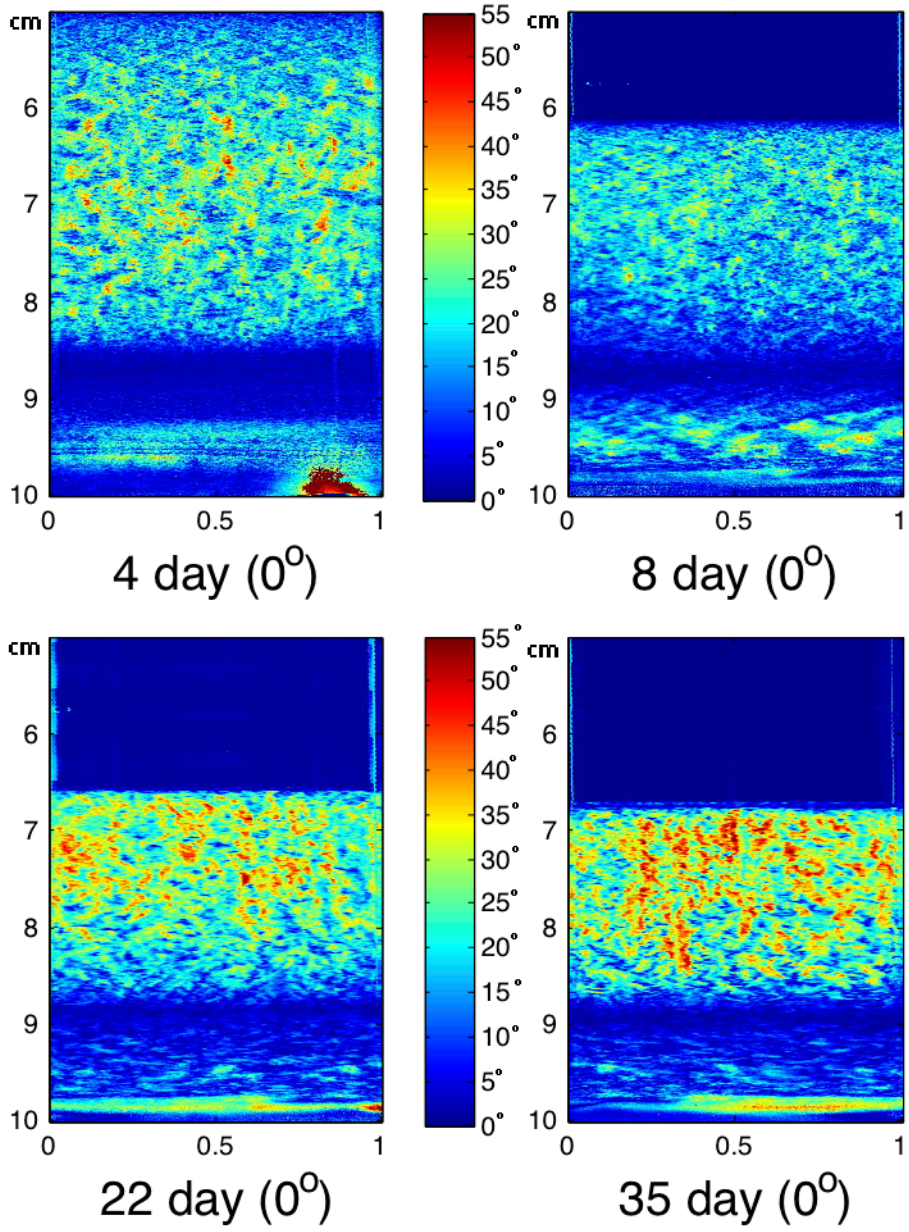

Figure 33: The degree of retardance of the bottom 5 cm of large unrotated uncentrifuged samples. First the retardance is sinking, while it is growing later. The units at the colorbars is degrees.

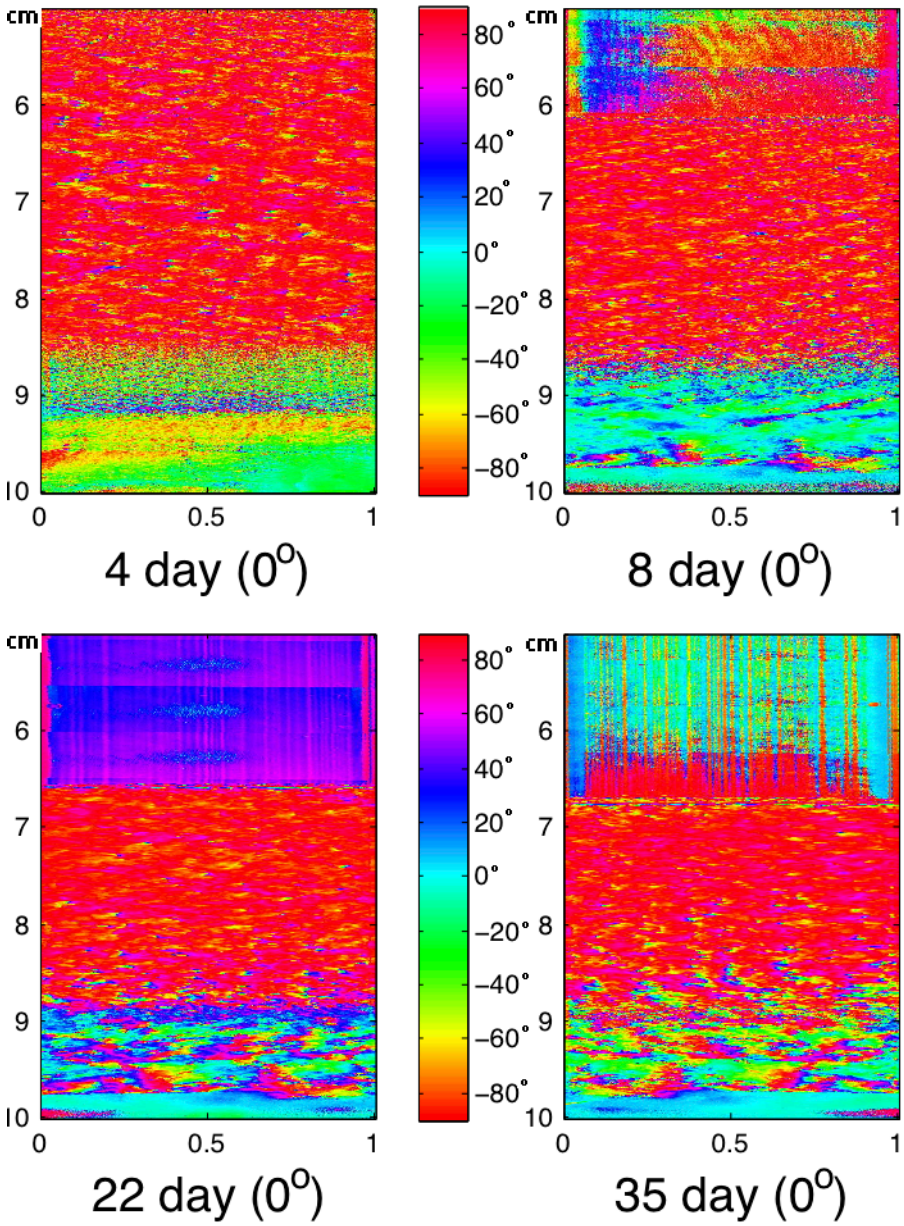

Figure 34: The direction of the fast axes of the retardance of the bottom half of large unrotated uncentrifuged samples. There are some artifacts from the isotropic phase, particularly in the last subfigure. The units at the colorbars is degrees.

8.3 Uncentrifuged clay, small and medium sample

The results for uncentrifuged clay in small and medium capillaries can be found in appendix A-1 and A-2. The phases develop in the same way as figure 31, while the depolarization and retardance are much weaker. Because of technical problems with the ellipsometer and leaky capillaries it was not possible to give a systematic surveys over its development. In appendix A-2 one can view an air bubble penetrate and destroying the bottom of the small capillary.

9 Outlook

The phenomenon of clay phases in aqueous dispersion, illustrated in this thesis through study of polarization states of light, is the foundation of understanding the properties of clay. The experiments and analyzes presented here are only the start of a new field of opportunities. Improving the ellipsometer could give new breakthrough. Among others the measurement time of the ellipsometer could be reduced in order to study the the early formation stages of the clay phases. Other ways to decompose the Mueller Matrices could also improve our understanding of clay. Symmetric decomposition could be better than forward decomposition when the problem of depolarization arise. Cloude decomposition could also be used to filtrate away unphysical Mueller matrices, resulting in better experimental results.

10 Conclusion

The thesis has discussed the theory behind Mueller matrices, in order to experimentally study the different phases of aqueous clay dispersions. The ellipsometer and Mueller matrices of air are also considered in order to understand the experimental results. Special attention were paid to the anisotropic phases, where the phenomena of retardance and depolarization were used to explore how the particles interacted with each other, liquids to liquids interfaces and the walls of the container. The result was improved understanding of the clay dispersion.

APPENDIX

A APPENDIX

A-1 Uncentrifuged clay, medium capillary

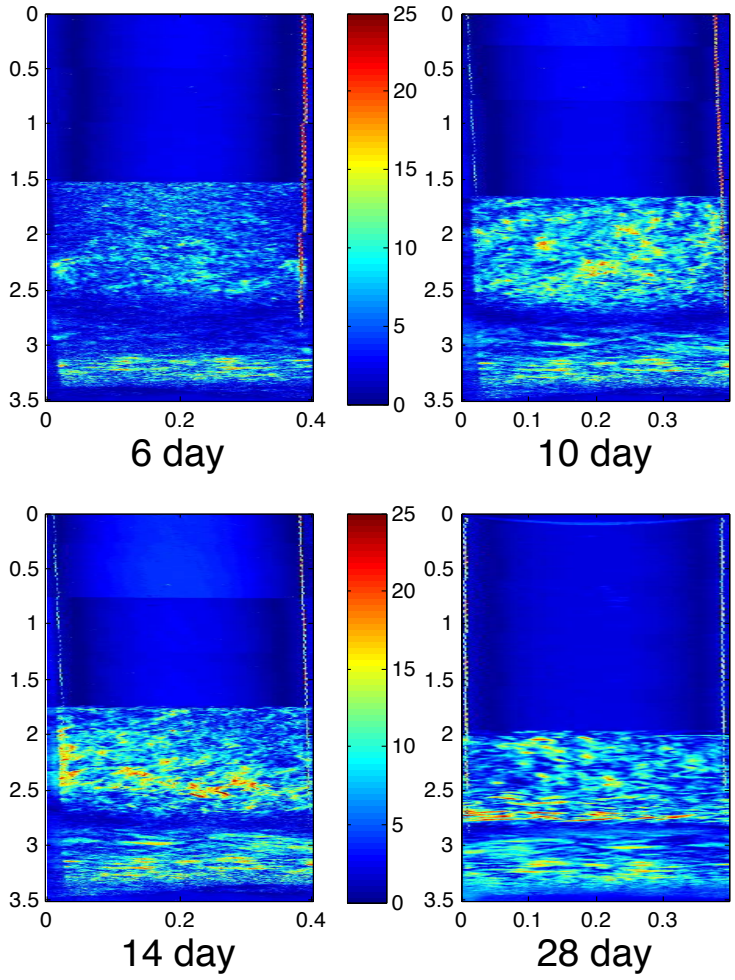

Figure 35: The development of the retardance of the uncentrifuged medium capillary.

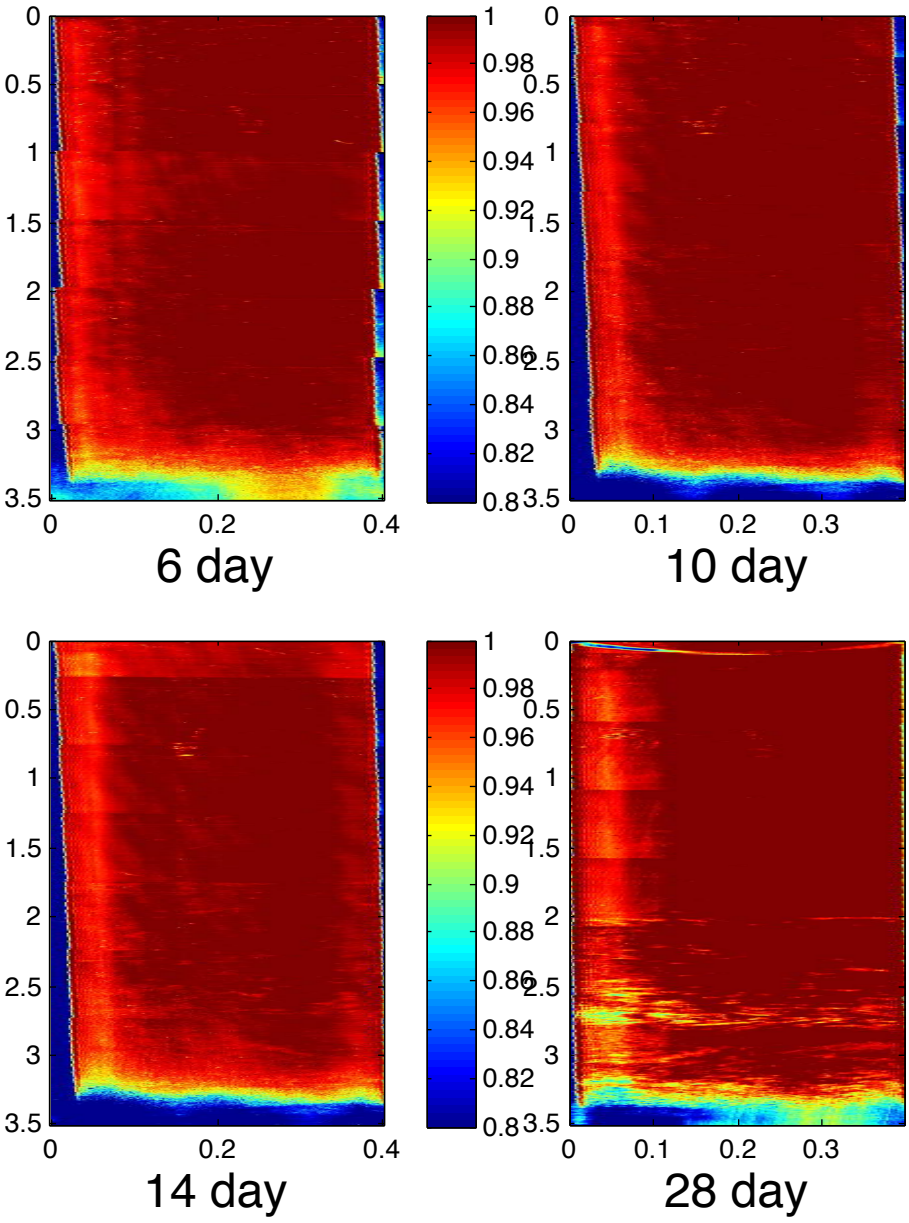

Figure 36: The development of the depolarization of the uncentrifuged medium capillary.

A-2 Uncentrifuged clay, small capillary

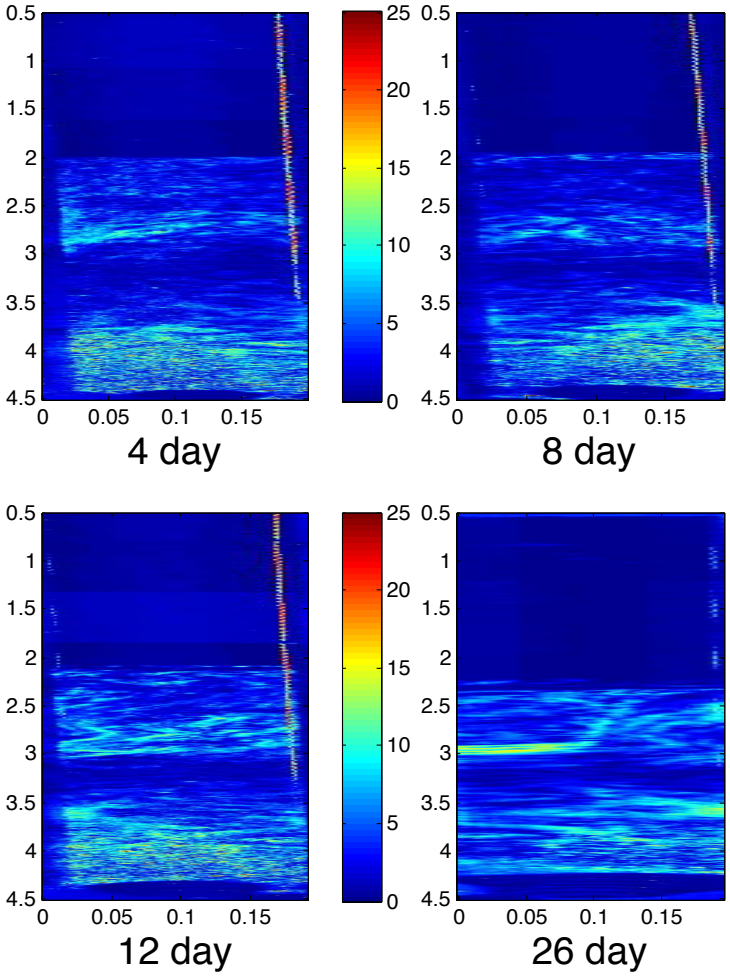

Figure 37: The development of the retardance of the uncentrifuged small capillary.

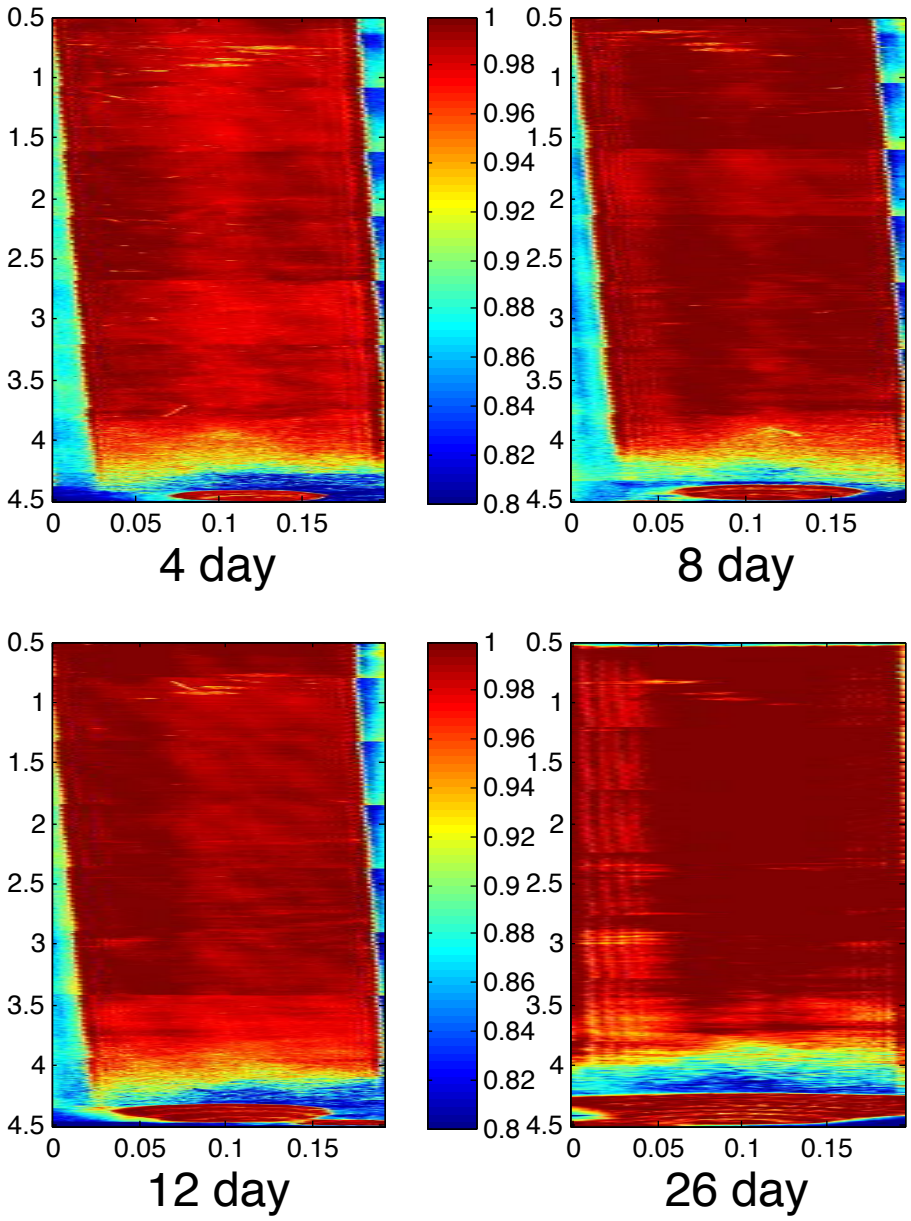

Figure 38: The development of the depolarization of the uncentrifuged small capillary.

References

[1] Dennis Goldstein. *Polarized Light. Marcel Dekker Inc., 2nd edition*, 2003. ISBN 0-8247-4053-X.

[2] Craig F. Bohren and Donald R. Huffman. *Absorption and scattering of light by small particles* 1983. ISBN 0-471-29340-7

[3] Shih-Yau Lu and Russell A. Chipman. Interpretation of Mueller matrices based on polar decomposition. *Journal of the Optical Society of America A*, 13(5),:11061113, 1996.

[4] Jerome Morio and Francois Goudail. Influence of the order of diattenuator, retarder and polarizer in polar decomposition of Mueller matrices. *Optics letter*, (29(19):2234-6, October 2004.

[5] S. Manhas, M. K. Swami, P. Buddhiwant, N. Gosh, P. K. Gupta and K. Singh. Mueller matrix approach for determination of optical rotation in chiral turbid media in backscattering geometry. *Opt. Express*, 14(1):190-202, 2006.

[6] R. Ossikovski, M. Anastasiadou, S. Ben Hatit, E. Garcia-Caurel and A. De Martino. Depolarizing Mueller matrices: how to decompose them? *phys. stat. sol.*, 205(4):720-727, 2008.

[7] R. Ossikovski, M. Anastasiadou, S. Ben Hatit, Steve Guyot and A. De Martino. Experimental validation of the reverse polar decomposition of depolarizing Mueller matrices. *Journal of the European Optical Society - Rapid publications*, Vol 2, 2007.

[8] Razvigor Ossikovski. Analysis of depolarizing Mueller matrices through a symmetric decomposition. *Journal of the Optical Society of America. A, Optics, image science and vision*, 26(5):1109-18, May 2009. ISSN 1084-7529

[9] J.J. Gil and E. Bernabeu. "Obtainment of the polarizing and retardation parameters of a non-depolarizing optical system from the polar decomposition of its Mueller matrix.". *Optik*, (Stuttgart) 76, 67-71 (1987)

[10] `http://www.adept.net.au/cameras/XenICs/XEVA-1.7-640.shtml`. 18.07.2011

[11] Pål Gunnar Ellingsen. *Development of Mueller matrix imaging technique for characterizing collagen spatial orientation in cartilage: comparison to multiphoton microscopy.* Master's thesis, NTNU, 2007.

[12] Lars Martin Sandvik Aas, Pål Gunnar Ellingsen, Morten Kildemo and Mikael Lindgren. *Journal of Modern Optics* Vol. 57, No. 17, 10 October 2010, 1603-1610.

[13] P. S. Hauge, R. H. Muller and C. G. Smith. Conventions and formulas for using the Mueller-Stokes calculus in ellipsometry. *Surface science*, 96(1-3):81107, 1980

[14] Elisabeth Lindbo Hansen 2010. *"Colloidal Dispersions of Clay Nanoplatelets" -Optical birefringence and x-ray scattering studies of nematic phases*. Master's thesis, NTNU, 2008

[15] Morten Kildemo, Lars. M. S. Aas, Pål G. Ellingsen, Henrik Hemmen, Elisabeth L. Hansen, Jon O. Fossum *"Mueller matrix imaging of nematic textures in colloidal dispersions of Na-fluorohectorite synthetic clay"*. NTNU, 2011.

[16] Erlend Granbo Rolseth. *Carbon Dioxide Intercalation in Sodium Fluorohectorite Clay*. Master's thesis, NTNU, 2011.

[17] J. O. Fossum, E. Gudding, D. M. Fonseca, Y. Meheust, E. DiMasi, T. Gog, and C. Venkataraman. "Gravity dispersed Clay colloids: Synchrotron x-ray Scattering Studies and Visual observations of oriental order in Na-Fluorohectorite Suspensions". *ENERGY The International Journal* 30, 873, 2005.

[18] J. O. Fossum, Y. Meheust, K. P. S. Parmar, K. D. Knudsen, K. J. Maløy and D. M. Fonseca. "Intercalation-enhanced electric polarization and chain formation of nano-layered particles". *Europhysics Letters* 74, 438, 2008.

[19] Asmae Khaldoun, Peder Moller, Abdoulaye Fall, Gerard Wegdam, Bert De Leeuw, Yves Meheust, Jon Otto Fossum and Daniel Bonn "Quick Clay and Landslides of Clayey Soils". *Phys. Rev. Lett.* 103, 188301, 2009.

[20] Henrik Hemmen, Nils I. Ringdal, Eduardo N. De Azevedo, Mario Engelsberg, Elisabeth L. Hansen, Yves Meheust, Jon O. Fossum and Kenneth D. Knudsen Langmuir "The Isotropic-Nematic Interface in Suspensions of Na-Fluorohectorite Synthetic Clay". *Langmuir*, 25(21), pp 12507-12515, 2009.

[21] D. van der Beek and H. N. W. Lekkerkerker. "Nematic ordering vs. gelation in suspensions of charged platelets.". *Europhys.* Lett. 61, 2003.